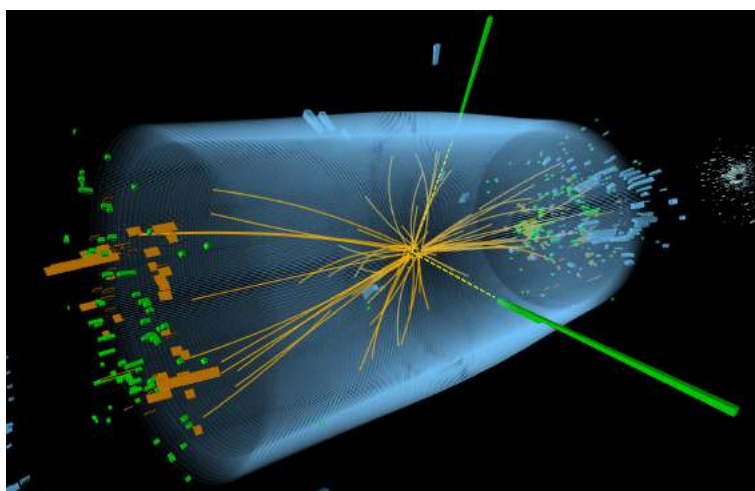


Evaluation of the Benefits of the CMS Electromagnetic Calorimeter Endcap LED Pulser to Improve the Stability of the Vacuum Phototriodes



Henry Aldridge

School of Physics and Astronomy

University of Southampton, UK

A dissertation submitted in partial fulfilment
for the degree of

Master of Particle Physics

May 2016

Acknowledgements

I would like to thank my supervisors Dave Cockerill and David Petyt for their guidance and support throughout this project. In addition I would like to thank the course coordinator Prof. Stefano Moretti and the University of Southampton, as well as Rutherford Appleton Laboratory, for arranging this course and giving me the opportunity to spend the year working at CERN.

Evaluation of the Benefits of the CMS Electromagnetic Calorimeter Endcap LED Pulser to Improve the Stability of the Vacuum Phototriodes

Henry Aldridge

Abstract

The vacuum phototriodes in the endcap electromagnetic calorimeter of the CMS detector are known to experience variations in response at the beginning and end of LHC fills. It is vital to minimise these variations to ensure that the electromagnetic calorimeter has the best resolution possible to detect and measure the energies of photons and electrons resulting from LHC collisions. Evaluations are made of the size of the variations and the benefits of the LED pulser system to minimise them. It was found that the average VPT step size plateaued to only reach 0.7% of the response, when photocathode currents increased as high as 1.3 nA. This is close to the physics requirement of minimising the impact on energy resolution to less than 0.5%. Steps have been observed to take place within four minutes of the end of LHC fills, which usually last more than eight hours. As a consequence, the VPT steps in response will only minimally affect physics at the LHC.

Contents

1	Introduction	1
2	CMS	5
2.1	Tracker	6
2.2	Electromagnetic Calorimeter	6
2.3	Hadronic Calorimeter	6
2.4	Magnet	7
2.5	Muon Detector and Return Yoke	7
3	ECAL	8
3.1	EE Geometry	8
3.1.1	Pseudorapidity	8
3.2	Lead Tungstate Crystals	9
3.3	Vacuum Phototriodes	10
3.3.1	High Voltage (HV) System	13
3.4	Laser Monitoring System	14
3.5	LED Pulser System	15
4	The Study of VPT Instabilities	17
5	VPT Photocathode Currents	19
5.1	CAEN Anode Currents	19
5.2	Estimating VPT Photocathode Currents	19
6	LHC Data For Analysis	21
6.1	Comparison Between Steps at the Beginning and End of Fills	21
6.2	Estimating Step Size	23
7	Step Size and VPT Position	25
8	Step Size and Instantaneous LHC Luminosity	31
9	Step Size and VPT Photocathode Current	34
9.1	Comparison Between Laboratory and LHC	36
10	Spread of Step Sizes	38
11	Conclusion	41
A	VPT Encoding	45
B	Data and Plot Generating Scripts	46

List of Figures

1.1	Feynman diagrams showing two important decay processes for the Higgs boson [3]. In both cases, the two gluons are involved in the collision between two protons. The gluons are linked to a top quark loop which couples with the Higgs field producing a Higgs boson. On the left, the Higgs boson subsequently decays into two photons through the Higgs decay to a top or bottom quark loop. On the right, two Z bosons are produced which each decay into two leptons.	1
1.2	Di-photon ($\gamma\gamma$) invariant mass distribution for the CMS data of 2011 and 2012 (black points with error bars). The data are weighted by the signal to background ratio for each sub-category of events. The solid red line shows the fit result for signal plus background; the dashed red line shows only the background [4].	2
1.3	Distribution of the four-lepton reconstructed mass for the sum of the $4e$, 4μ , and $2e2\mu$ channels. Points represent the data, shaded histograms represent the background and un-shaded histogram the signal expectations. The distributions are presented as stacked histograms. The measurements are presented for the sum of the data collected at centre of mass energies of 7 TeV and 8 TeV [4].	3
1.4	Event recorded in the CMS detector in 2012. It is characteristic of the standard model Higgs boson decay into two photons (dashed yellow lines and green lines) [5].	3
1.5	Event recorded in the CMS detector in 2012. It is characteristic of the standard model Higgs boson decay into two Z bosons, one of which then decays into two electrons (green lines) and the other decays into two muons (red lines) [6].	4
1.6	Example of steps at the beginning and end of an LHC fill, for channel (41,41) on 13th October 2011. Response was normalised to the beginning of operation in 2011. The shaded red areas show the periods of LHC fill with collisions. The white regions are periods where the LHC is off.	4
2.1	Diagram of the CMS detectors with the Tracker, ECAL, HCAL, Magnet and Muon Detector [9].	5
2.2	Transverse slice through CMS showing the path of muons, electrons, charged hadrons, neutral hadrons and photons through the detector [10].	6
3.1	Diagram of the CMS electromagnetic calorimeter, with the the endcaps, the preshower, and the crystal supermodules in the barrel [11].	9
3.2	A single ECAL Endcap with the Dees apart. Each block represents a supercrystal [12].	10
3.3	Picture of an endcap Dee [11].	11
3.4	Diagram showing example of relative angle, θ between the beam axis, the interaction point, and a crystal and VPT.	11
3.5	An example of a lead tungstate (PbWO_4) crystal used in the CMS ECAL with a VPT glued to its rear face	12
3.6	Producers of crystals used in EE+. Red crystals are Chinese (SIC) and green are Russian (BTCF)	12
3.7	Diagram showing the dimensions inside a VPT [17]. The VPT has a length of 40 mm, with the photocathode, anode and dynode located within the front 4.5 mm.	13

3.8	An example of a VPT used in the endcaps of the CMS ECAL.	14
3.9	ECAL laser monitoring system. The light source and high-level distribution system feed into a two-level distribution system to supply light to each crystal in the ECAL [12]. . .	15
3.10	The laser response history of the ECAL in 2011 and 2012. The top graph shows the average relative response, normalised to the beginning of operation in 2011, for crystal/VPT channels in particular bands of pseudorapidity. The bottom plot shows the instantaneous LHC luminosity over the same time period [18]. The three shaded areas are October 2011, May 2012 and December 2012 which were the three time periods used in this project.	16
3.11	Schematic diagram showing the distribution system for the ECAL LED pulser system [11].	16
4.1	Average normalised response of 200 production VPTs for an LHC simulation at 0 T (open circles) and 3.8 T (filled circles). A pulse load of 10 kHz was supplied for 17 hours and turned off at T=0 hours. The VPT response was normalised to T=-10 hours [19]. .	18
4.2	Laboratory measurement of the response of CMS VPT 2181 against time for simulated LHC on/off cycles with soak light at 0 Hz (left) and 100 Hz (right). Red points represent LHC on and blue LHC off.	18
5.1	CAEN HV current measurements from CMSWBM for Dee 1 Ch 2 on 16th-17th October 2011. The HV current is in units of μA	20
6.1	Pulsed and unpulsed regions of EE+ in October 2011 and December 2012 (Red is pulsed, blue is unpulsed). The pulsed regions comprise 6539 crystals and the unpulsed regions comprise 785.	22
6.2	Instantaneous luminosities ($10^{30} \text{ cm}^{-2} \text{ s}^{-1}$) against date for the LHC fills in October 2011	22
6.3	Instantaneous luminosities ($10^{30} \text{ cm}^{-2} \text{ s}^{-1}$) against date for the LHC fills in December 2012	23
6.4	Instantaneous luminosities ($10^{30} \text{ cm}^{-2} \text{ s}^{-1}$) against date for the LHC fills in May 2012.	23
6.5	Response of channel (41,41) normalised to the beginning of 2011, against date. The shaded red areas show the periods of LHC fills with collisions. The white regions are periods where the LHC is off.	24
7.1	The average step size for pulsed (red) and unpulsed (blue) VPTs and the VPT photocathode current (magenta) at the end of the first fill in the October 2011 set against η . The final LHC luminosity was approximately $1.5 * 10^{33} \text{ cm}^{-2} \text{ s}^{-1}$. The left-hand vertical axis shows the VPT step size as a percentage of the VPT response at the end of the fill. The right-hand vertical axis shows VPT photocathode current in nA.	27
7.2	The average step size for pulsed (red) and unpulsed (blue) VPTs and the VPT photocathode current (magenta) at the end of the first fill in the December 2012 set against η . The final LHC luminosity was approximately $3 * 10^{33} \text{ cm}^{-2} \text{ s}^{-1}$. The left-hand vertical axis shows the VPT step size as a percentage of the VPT response at the end of the fill. The right-hand vertical axis shows VPT photocathode current in nA.	28
7.3	The average absolute step size for pulsed (red) and unpulsed (blue) VPTs, and the VPT photocathode current (magenta), at the end of the first fill in the December 2012 set against η . The end-of-fill LHC luminosity was approximately $3 * 10^{33} \text{ cm}^{-2} \text{ s}^{-1}$. The left-hand vertical axis shows the absolute VPT step size, where the VPT response has been normalised to the beginning of 2011. The right-hand vertical axis shows the VPT photocathode current at the end of the fill.	29
7.4	Response of channel (50,39) normalised to the beginning of 2011, against date. Shaded red areas are LHC on and white are LHC off. Red lines show the linear fit to the data towards the end of each fill. The end of fill percentage step sizes vary from 0.15% to 0.45%. 30	30

8.1	The LHC instantaneous luminosity (displayed in units of $10^{30} \text{ cm}^{-2} \text{ s}^{-1}$) in red, and anode current (μA) in blue, against time for 16-17th October 2011. The anode current shown is for Dee 1, channel 2 of EE+. The current has a baseline of $365.5 \mu\text{A}$. The measurement precision is $0.5 \mu\text{A}$. The system updates after a change larger than $0.5 \mu\text{A}$.	32
8.2	Mean and RMS of step size against luminosity ($10^{30} \text{ cm}^{-2} \text{ s}^{-1}$) for radius 0.31-0.40 m. Step size is as a percentage of response at end of fill. Magenta square, blue triangular and red circular points correspond to October 2011, May 2012 and December 2012 respectively. Inset graph shows which VPTs were used in black.	32
8.3	Mean and RMS of step size against luminosity ($10^{30} \text{ cm}^{-2} \text{ s}^{-1}$) for radius 0.31-0.40 m in October 2011. Step size is as a percentage of response at end of fill. Inset graph shows which VPTs were used (red are pulsed, blue are unpulsed).	33
8.4	Mean and RMS of step size against luminosity ($10^{30} \text{ cm}^{-2} \text{ s}^{-1}$) for radius 0.31-0.40 m in May 2012. Step size is as a percentage of response at end of fill. Inset graph shows which VPTs were used. All VPTS were unpulsed. Red points were pulsed in October 2011 and December 2012, blue were not.	33
9.1	Absolute step size against end of fill VPT photocathode current for October 2011 (magenta), May 2012 (blue) and December 2012 (red). The VPTs were pulsed in October 2011 and December 2012 but not in May 2012. VPT photocathode current has units of nA. The response of each channel was normalised to the beginning of operation in 2011. Only the VPTs that were pulsed in October 2011 and December 2012 have been used.	35
9.2	Percentage step size against end of fill VPT photocathode current for October 2011 (magenta), May 2012 (blue) and December 2012 (red). The VPTs were pulsed in October 2011 and December 2012 but not in May 2012. VPT photocathode current has units of nA. The step size is as a percentage of the response of the channel at the end of fill. Only the VPTs that were pulsed in October 2011 and December 2012 have been used.	36
9.3	Absolute step size against end of fill VPT photocathode current for October 2011 for pulsed (red) and unpulsed (blue) VPTs. VPT photocathode current has units of nA. The response of each channel was normalised to the beginning of operation in 2011.	36
9.4	Absolute step size against end of fill VPT photocathode current for December 2012 for pulsed (red) and unpulsed (blue) VPTs. VPT photocathode current has units of nA. The response of each channel was normalised to the beginning of operation in 2011.	37
10.1	Spread of absolute step sizes for pulsed (left, red) and unpulsed (right, blue) VPTs for the fills investigated in October 2011, May 2012 and December 2012. The response of each channel was normalised to the beginning of operation in 2011.	38
10.2	Percentage step size against end-of-fill photocathode current for the VPT at (59,67) in EE+. Pulsed points, from October 2011 and December 2012, are red. Unpulsed points, from May 2012 are blue. Step size is as a percentage of the channel's response at the end of the fill.	39
10.3	Absolute step size against end-of-fill photocathode current for the VPT at (59,67) in EE+. Pulsed points, from October 2011 and December 2012, are red. Unpulsed points, from May 2012 are blue. The response of the channel was normalised to the beginning of operation in 2011.	40

1

Introduction

The Large Hadron Collider (LHC) at CERN is a high-energy particle accelerator built with the purpose of searching for new physics and testing the predictions from the standard model, such as the Higgs, supersymmetry and dark matter. The most notable recent discovery, as announced by both the ATLAS [1] and CMS [2] experiments on the LHC, was the Higgs boson: the final elementary particle predicted by the standard model.

The Higgs boson was observed through various decay processes, two of which are $H \rightarrow \gamma\gamma$ and $H \rightarrow ZZ^* \rightarrow 4L$. Feynman diagrams for these processes are shown in Figure 1.1, on the left and right respectively. The four leptons (L) can be either four electrons (e), four muons (μ), or two electrons and two muons. The CMS electromagnetic calorimeter (ECAL) was crucial for the detection of the resultant photons (γ) and electrons to confirm the existence of the Higgs boson and will continue to be important for future physics results. Figures 1.2 and 1.3 show results from CMS which indicate the presence of the Higgs boson and Figures 1.4 and 1.5 show an example of one of these events.

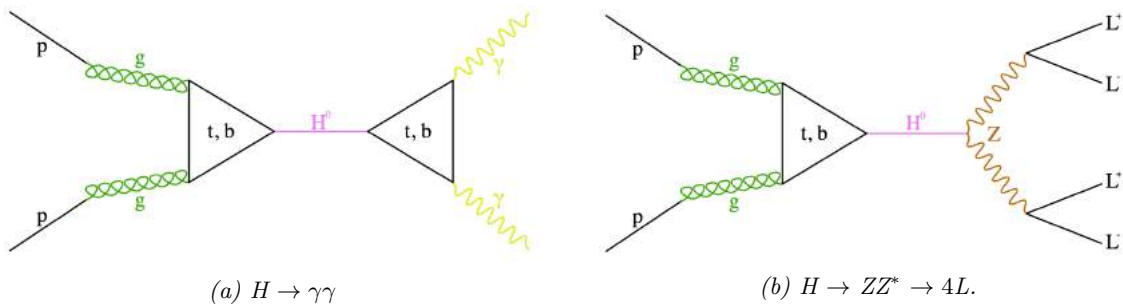


Figure 1.1: Feynman diagrams showing two important decay processes for the Higgs boson [3]. In both cases, the two gluons are involved in the collision between two protons. The gluons are linked to a top quark loop which couples with the Higgs field producing a Higgs boson. On the left, the Higgs boson subsequently decays into two photons through the Higgs decay to a top or bottom quark loop. On the right, two Z bosons are produced which each decay into two leptons.

The Compact Muon Solenoid (CMS) is one of two general purpose detectors on the LHC. The elec-

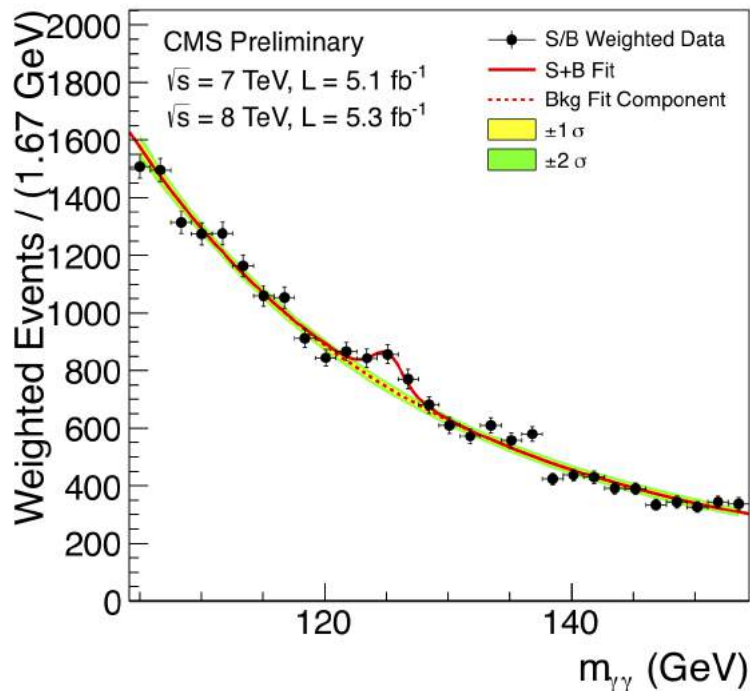


Figure 1.2: Di-photon ($\gamma\gamma$) invariant mass distribution for the CMS data of 2011 and 2012 (black points with error bars). The data are weighted by the signal to background ratio for each sub-category of events. The solid red line shows the fit result for signal plus background; the dashed red line shows only the background [4].

tromagnetic calorimeter (ECAL) comprises 75848 lead tungstate (PbWO_4) crystals split between the barrel and two endcaps (EE). At the rear face of each crystal is a photomultiplier, which is an avalanche photodiode (APD) in the barrel and a vacuum phototriode (VPT) in the endcaps. It is vital that the ECAL has the best possible energy resolution [7]. The aim of the ECAL is to measure photon and electron energies with a resolution of 0.5% for energies above 100 GeV.

However, there is a concern that instabilities in the VPTs used in endcaps of ECAL could affect the resolution and the overall response of the detector. VPT instabilities are particularly apparent at the beginning and end of the LHC fills. This is due to the large changes in instantaneous LHC luminosity as a LHC fill begins or ends, resulting in large light load variations on the VPTs. Figure 1.6 shows an example of the consequent steps in response seen on a channel in CMS.

In laboratory conditions ‘steps’ in the response of VPTs at the beginning and end of simulated LHC fills were observed at approximately 1.7% of their total response. These steps were reduced to 0.7% in some cases using an LED pulser system to provide a constant background to stabilise the VPTs [8]. The purpose of this project was to determine whether these instabilities are seen with real LHC data in the ECAL and whether the LED pulser system is effective in reducing them.

To investigate the step sizes, data from a number of sources are needed and each of these are explained in more detail in this report. A laser monitoring system is used to track the response of each channel. A channel consists of a crystal and VPT. The laser monitoring data is used to calculate the steps in response which are the subject of this report. LHC luminosity data is used to determine the beginning and end times of each LHC fill and also to compare step sizes and instantaneous LHC luminosity. This data is taken from the CMS web-based monitoring system (CMSWBM). A CAEN high voltage system is used to distribute high voltages to the anode and dynode of each VPT. A measurement of the

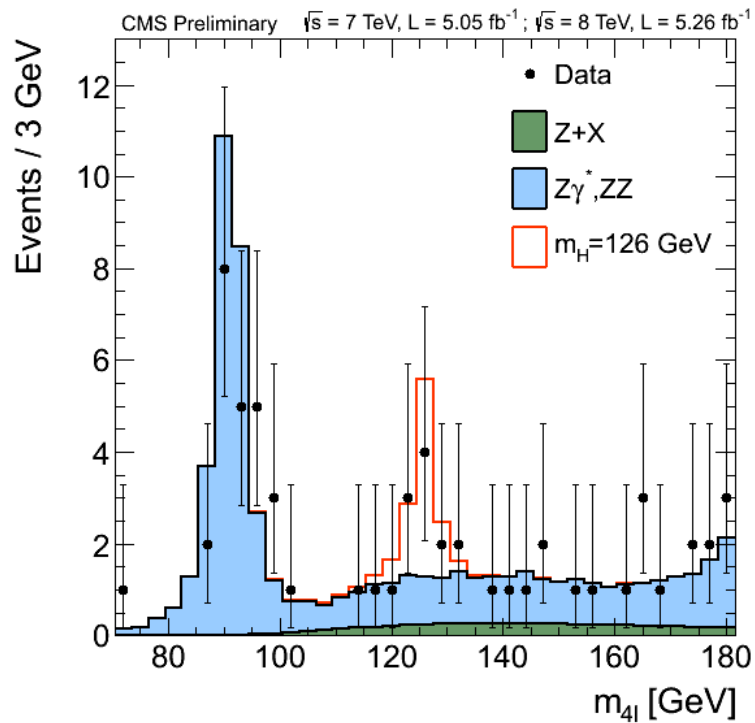


Figure 1.3: Distribution of the four-lepton reconstructed mass for the sum of the $4e$, 4μ , and $2e2\mu$ channels. Points represent the data, shaded histograms represent the background and un-shaded histogram the signal expectations. The distributions are presented as stacked histograms. The measurements are presented for the sum of the data collected at centre of mass energies of 7 TeV and 8 TeV [4].

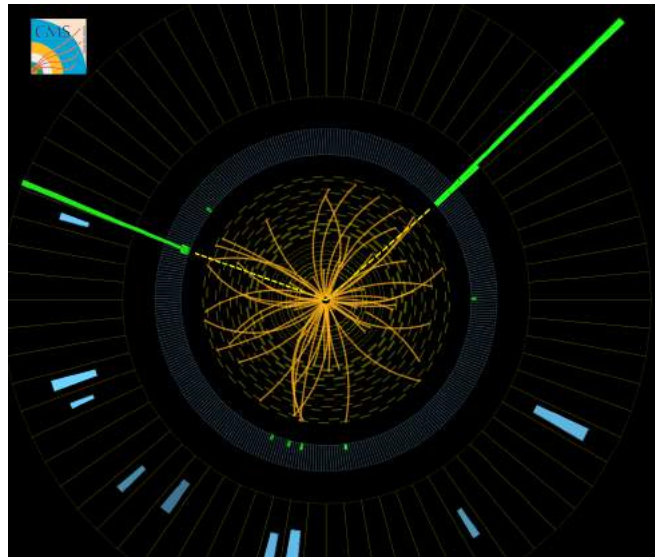


Figure 1.4: Event recorded in the CMS detector in 2012. It is characteristic of the standard model Higgs boson decay into two photons (dashed yellow lines and green lines) [5].

anode currents allow an estimate of VPT photocathode currents to be made. These represent the load experienced by a VPT. The anode current data are also taken from CMSWBM.



Figure 1.5: Event recorded in the CMS detector in 2012. It is characteristic of the standard model Higgs boson decay into two Z bosons, one of which then decays into two electrons (green lines) and the other decays into two muons (red lines) [6].

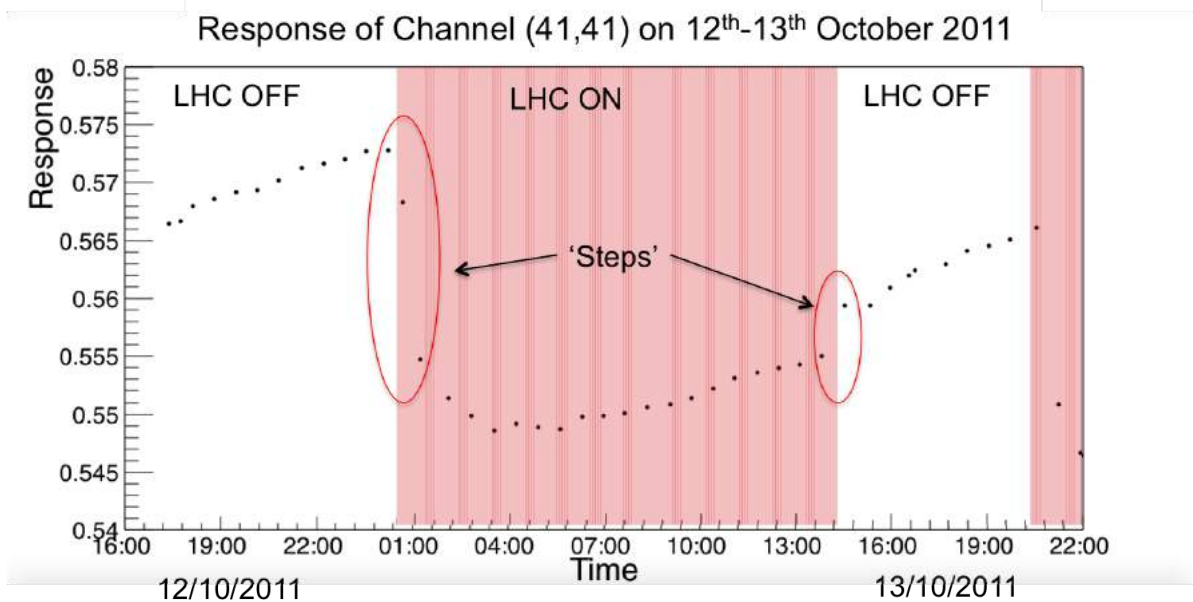


Figure 1.6: Example of steps at the beginning and end of an LHC fill, for channel (41,41) on 13th October 2011. Response was normalised to the beginning of operation in 2011. The shaded red areas show the periods of LHC fill with collisions. The white regions are periods where the LHC is off.

2

CMS

CMS is shown in Figures 2.1 and 2.2 and is one of two general purpose detectors at the LHC. The detector is 21.6 m in length and 15 m in diameter, operating with a 3.8 T magnetic field. It consists of a barrel section and two endcaps. CMS has five distinct sub-detectors, each with a different purpose: the tracker, followed by the electromagnetic calorimeter (ECAL), the hadronic calorimeter (HCAL), the magnet and finally the muon detector and return yoke.

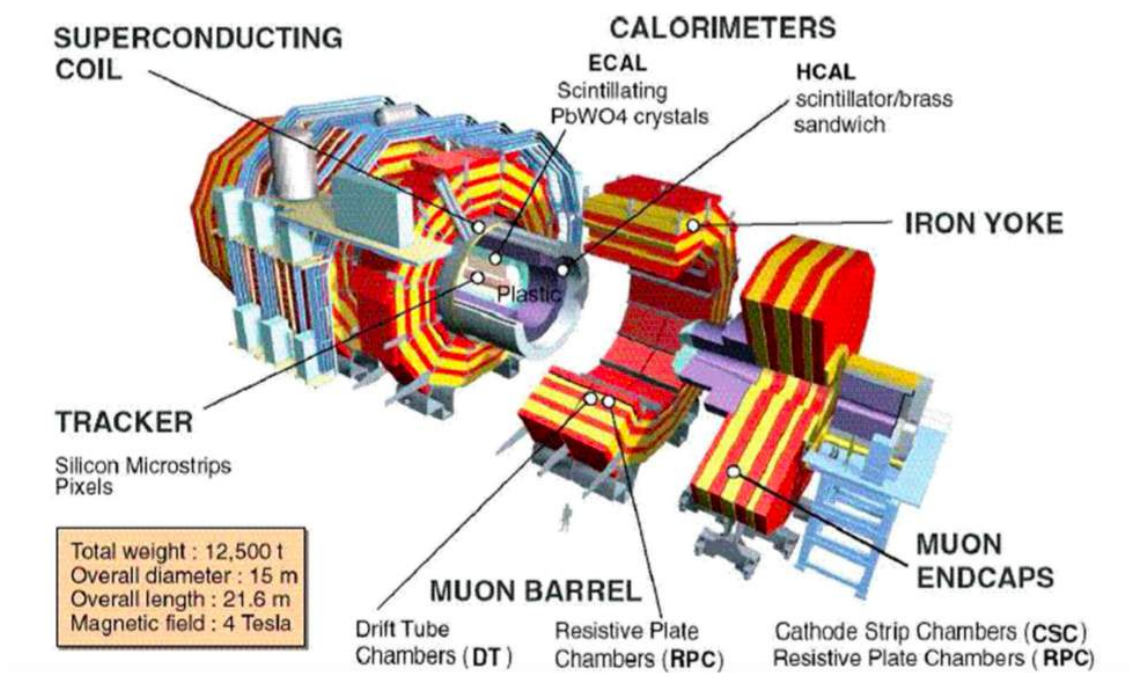


Figure 2.1: Diagram of the CMS detectors with the Tracker, ECAL, HCAL, Magnet and Muon Detector [9].

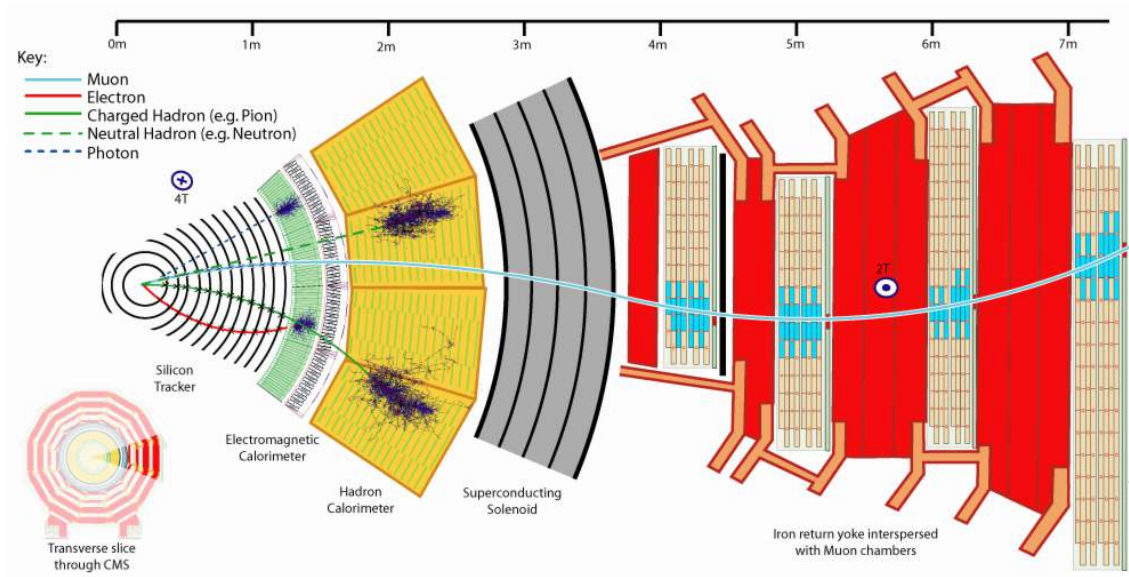


Figure 2.2: Transverse slice through CMS showing the path of muons, electrons, charged hadrons, neutral hadrons and photons through the detector [10].

2.1 Tracker

The tracker consists of silicon pixels and silicon microstrips which record the position of charged particles as they traverse the tracker volume. From the curvature of the charged particle trajectory in the 3.8 T magnetic field, the momenta of the charged particles can be calculated.

The tracker is also used to detect secondary vertices, for example from b-decays, and to identify jets of charged particles travelling in proximity to each other.

2.2 Electromagnetic Calorimeter

The purpose of the ECAL is to detect and measure the energies of photons and electrons. It consists of 75848 lead tungstate crystals with a photomultiplier at the rear face of each. The level of crystal scintillation is proportional to the energy of the photon or electron entering it. The ECAL, specifically its endcaps, were the focus of this project and the relevant parts are described in more detail in the next section.

2.3 Hadronic Calorimeter

The HCAL measures the energies of hadrons such as pions, protons and neutrons. It is a sampling calorimeter consisting of layers of brass or steel interleaved with plastic scintillators. Wavelength-shifting fibres are used to efficiently collect the scintillation photons and convert the light to wavelengths with a suitable match to the hybrid photodiode detectors. The hadronic forward detector (HF) uses steel absorbers and quartz fibres for readout. This provides a radiation robust system for this high radiation region.

2.4 Magnet

The superconducting solenoid magnet produces a 3.8 T magnetic field and is made from niobium-titanium coils. The magnetic field curves the tracks of charged particles in the detector. The 3.8 T field requires an operating current of 18160 A, and has a stored energy of 2.3 GJ.

2.5 Muon Detector and Return Yoke

The muon detector is the last of the CMS subsystems. Muons are charged leptons. Their interaction with CMS via the weak force are negligible. Their interactions via the electromagnetic force are also minimal and are limited to small ionisation losses and occasional bremsstrahlung which goes as $1/m_\mu^2$. As a consequence they can pass through the rest of the CMS detector with minimal interactions. Three types of detector are used in the muon detector: drift tubes (DT), cathode strip chambers (CSC) and resistive plate chambers (RPC). The DTs are used in the barrel for precise trajectory measurements. The drift tube is a tube containing a stretched wire in a gaseous volume. A muon passing through knocks electrons off the atoms in the gas. They are accelerated to the positively charged wire. The position of the electrons on the wire and the time taken for the electron to contact the wire allows for two coordinates of the muon's position to be determined. The DTs form a grid, allowing the precise position and momentum of a muon to be determined.

The CSCs are used in the endcaps because there is a less even magnetic field and higher particle rates. They consist of positively charged anode wires crossed with negatively charged cathode strips. They operate in a similar way to DTs but use a grid of positively charged anode wires and negatively charged cathode strips instead of a single wire.

RPCs are used in both the barrel and the endcaps and comprise an anode plate and a cathode plate, again in a gas volume. When a muon enters the chamber, it liberates an electron avalanche in the gas which is then detected. This provides a rapid signal which the trigger uses to decide whether the data is worth keeping.

These components are located within the iron return yoke which is a 12-sided iron structure which contains and guides the magnetic field.

3

ECAL

The ECAL consists of a cylindrical barrel and two endcaps, with 61200 lead tungstate (PbWO_4) crystals in the barrel and 7324 in each endcap. There are two endcaps; the positive endcap (EE+) and the negative endcap (EE-). This project focused on EE+.

3.1 EE Geometry

Each endcap is constructed of two semicircular ‘Dees.’ Each block within the Dee is a ‘supercrystal’ with a 5x5 group of crystals. Supercrystals on the inner and outer edges have fewer than 5x5.

A diagram of an endcap showing the two Dees and the supercrystals is in Figure 3.2. It also gives an indication of the pseudo-projective geometry of the crystals in the endcap towards the interaction point. Figure 3.3 shows a photograph of a Dee.

In each endcap the VPTs have an i_x and i_y value ranging from one to 100. The i_z value is +1 or -1, where +1 corresponds to EE+ and -1 to EE-. Each combined crystal and VPT in the EE is identified by a unique eight digit hexadecimal ID number for that channel. The formula to extract the locations can be found in Appendix A.

3.1.1 Pseudorapidity

Pseudorapidity (η) is a spatial coordinate commonly used in experimental particle physics and is used in this report to describe the location of VPTs. Equal intervals or rapidity receive equal levels of particle energy flow. Higher η values receive more radiation per physical unit area. Figure 3.4 shows the positioning between the interaction point, beam axis, and a crystal and VPT.

The pseudorapidity, η , of the crystal and VPT shown in Figure 3.4 is given by equation 3.1.

$$\eta = -\ln\left(\tan\frac{\theta}{2}\right) \tag{3.1}$$

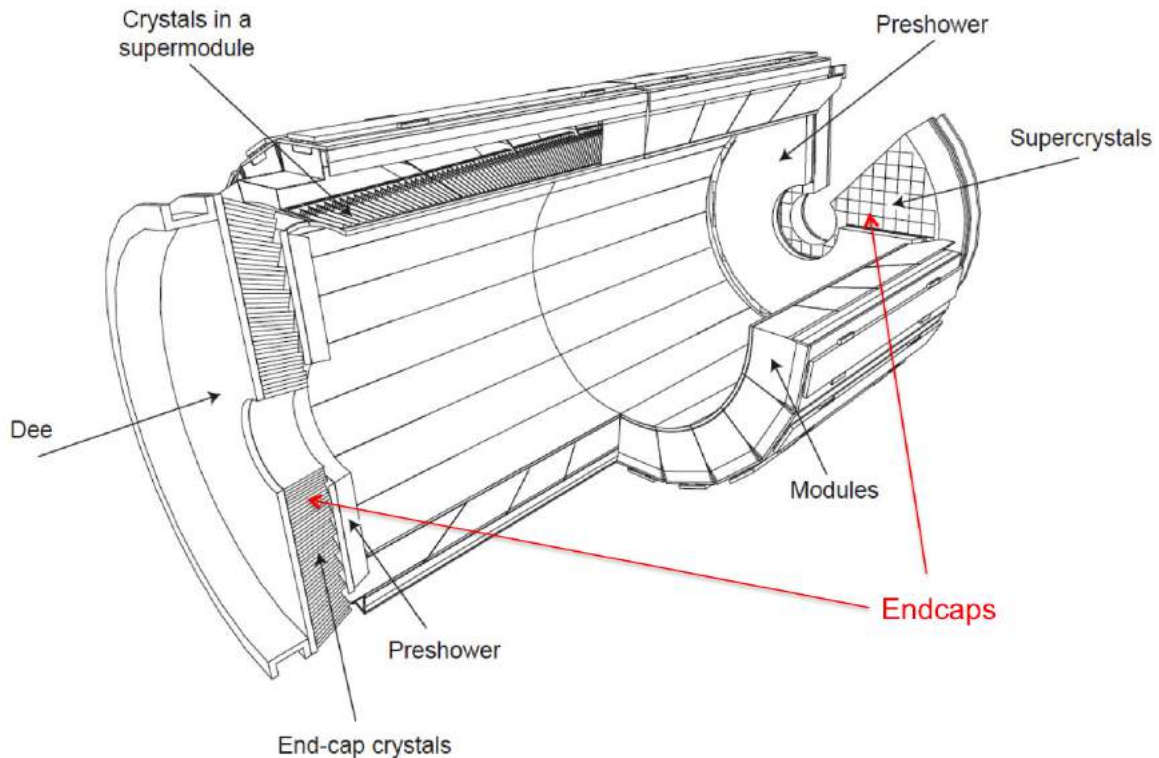


Figure 3.1: Diagram of the CMS electromagnetic calorimeter, with the the endcaps, the preshower, and the crystal supermodules in the barrel [11].

where θ is the relative angle between the beam axis and the crystal and VPT.

The barrel ECAL covers a pseudorapidity range of $-1.48 < \eta < 1.48$. The endcaps cover a pseudorapidity range of $1.48 < \eta < 3.0$, corresponding to the outer and inner regions of the EE respectively.

3.2 Lead Tungstate Crystals

The lead tungstate (PbWO_4) crystals used in the ECAL are grown from a 50%-50% mixture of lead oxide (PbO) and tungsten oxide (WO_3). The crystals have been chosen because they have properties which are important for the ECAL. They emit scintillation light quickly, with 80% emitted within 25ns. This prevents overlapping signals in a crystal from two separate LHC collisions. The crystals' short radiation length and Moliere radius allow for a compact calorimeter [13]. Additionally they have a scintillation emission at 420nm, with a good match to the quantum efficiency of both the APDs and the VPTs [12]. The crystals are 220 mm in length and have a cross section of approximately $30 \times 30 \text{ mm}^2$ [14]

High energy electrons or photons entering lead tungstate (PbWO_4) crystals cause an electromagnetic shower of particles to be produced. The charged particles in the shower cause the crystals to scintillate, at a level proportional to the energy of the incoming electron or photon. These photons then enter APDs in the barrel, or VPTs in the endcaps, at the rear of the crystals where they are converted to an electrical current and amplified for detection.

The EE crystals suffer from radiation damage. This damage causes colour centres to form during LHC fills, resulting in a loss of transparency. The radiation-induced self-absorption of the light in the

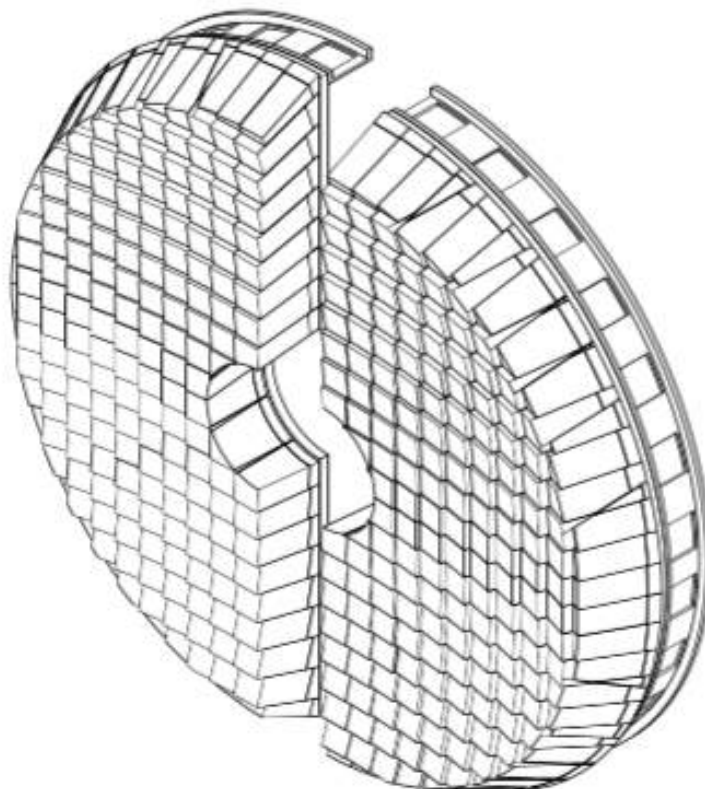


Figure 3.2: A single ECAL Endcap with the Dees apart. Each block represents a supercrystal [12].

crystals reduces their transmission. The colour centres recover through annealing at room temperature [12].

Further damage is caused by collisions between high-energy hadrons and the nuclei. The highly charged ions produced in the resulting fission travel through the crystal, disrupting the lattice and creating permanent colour centres.

There are two manufacturers of the crystals used in EE+. The majority of crystals used are Russian (BTCP) and a small number, on the inner and outer edges of the endcap, are Chinese (SIC). Figure 3.6 shows the distribution of crystals.

3.3 Vacuum Phototriodes

VPTs are used for the EE because they are more radiation-tolerant than APDs. This is especially important in the higher pseudorapidity region in EE [12].

The VPTs are 40 mm in length with a diameter of 26.5 mm and have a UV glass window with an active area of 280 mm^2 [13]. A photocathode is situated at the faceplate, followed by a mesh anode and then a dynode, as shown in Figure 3.7. Photoelectrons are released from the photocathode when struck by scintillation photons. The photocathode is held at ground potential. Approximately half of the photoelectrons pass through the mesh anode to reach the dynode which is held at +600 V. For each of these electrons, approximately 20 secondary electrons are emitted from the dynode. Half are collected on the anode, which is held at +800 V, to form the VPT signal.



Figure 3.3: Picture of an endcap Dee [11].

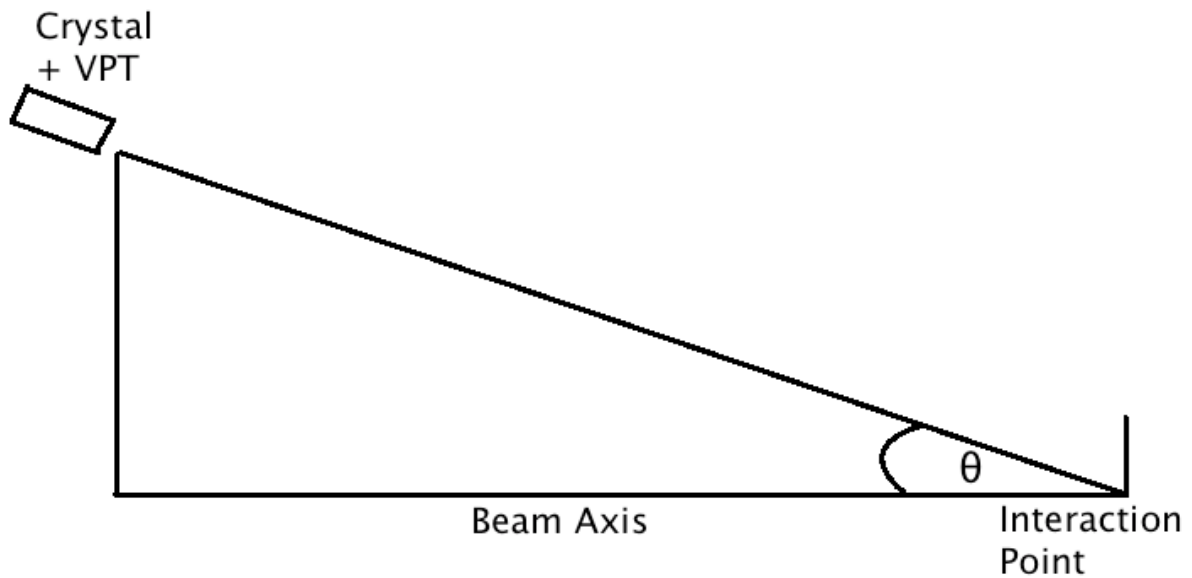


Figure 3.4: Diagram showing example of relative angle, θ between the beam axis, the interaction point, and a crystal and VPT.

The VPTs have a gain of approximately 8-10 and a quantum efficiency of approximately 20% at 420 nm which matches the scintillation emission of the lead tungstate crystals.

A very fine anode mesh with a pitch of $10 \mu\text{m}$ is used to provide a level of immunity to the 3.8 T magnetic field. The anode is in close proximity to both the photocathode and the dynode. The anode mesh has a transparency of 50%. Half of the photoelectrons pass through the anode and impact the dynode. Secondary electrons from the dynode are collected on the anode to provide the main signal



Figure 3.5: An example of a lead tungstate ($PbWO_4$) crystal used in the CMS ECAL with a VPT glued to its rear face

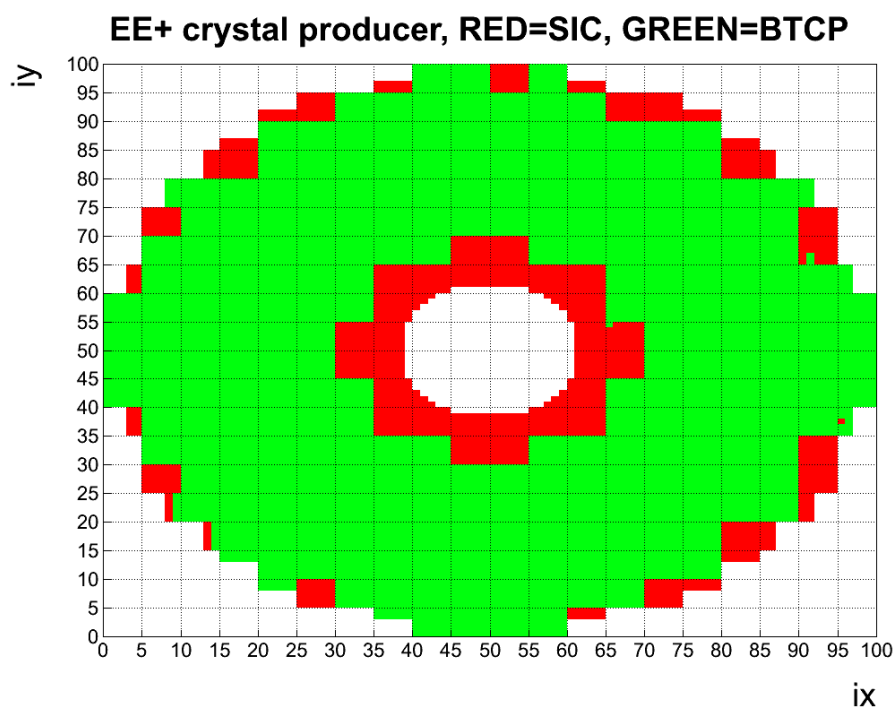


Figure 3.6: Producers of crystals used in EE+. Red crystals are Chinese (SIC) and green are Russian (BTCP)

from the VPT. About 20 secondary electrons are emitted for each electron impacting the dynode. Half of these will be collected on the anode.

The mesh anode VPTs used in the endcaps are radiation-resistant but suffer both short and long term effects. Long term effects, over weeks, concern darkening of the faceplates and photocathode degradation. Accelerated electrons collide with residual gases in the VPT, ionising them. These ions are then accelerated towards the photocathode where they collide and cause damage to the photocathode [15].

The focus of this project, however, was on the short term changes in response in the space of under four minutes which occur due to the light load variations on the VPTs in LHC operation cycles. These changes, called ‘steps,’ are particularly apparent at the start and end of LHC fills, as the total luminosity suddenly changes from zero to $10^{34} \text{ cm}^{-2} \text{ s}^{-1}$. A laser monitoring system takes measurements every 40 minutes to allow for corrections to be made but the VPT steps in response take less time than this. This causes issues because the laser system cannot track, and correct for, such short steps in response. This could lower the resolution of the detector and may result in less accurate and reliable data during this period.

Previous work has shown that VPT instabilities were reduced by a factor of ten in the 3.8 T CMS magnetic field compared to the instabilities seen without the calming effect of the field, at 0 T [16]. However, in the laboratory, even with a 3.8 T field, the step instabilities are still seen and are the subject of this report.

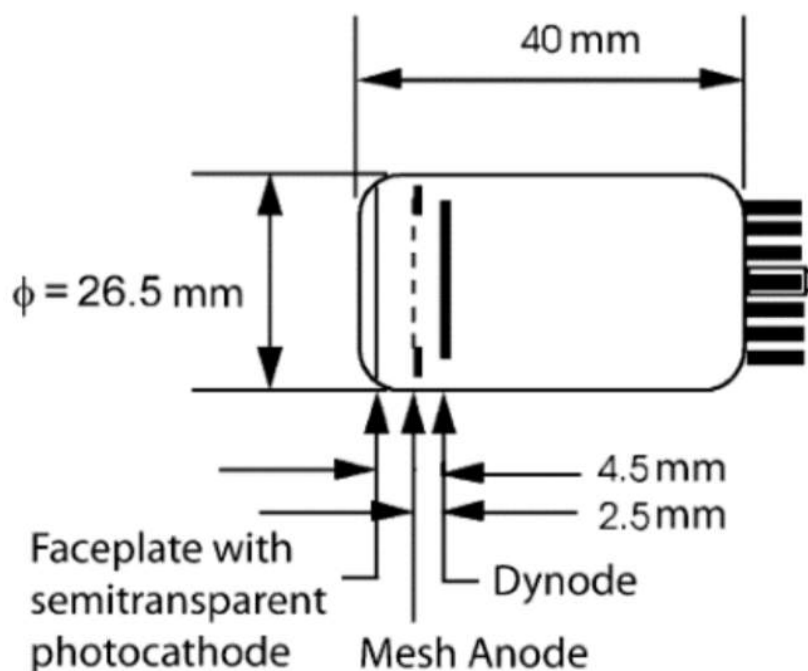


Figure 3.7: Diagram showing the dimensions inside a VPT [17]. The VPT has a length of 40 mm, with the photocathode, anode and dynode located within the front 4.5 mm.

3.3.1 High Voltage (HV) System

To supply the two voltages (+600 V dynode and +800 V anode) to each VPT, a high voltage (HV) system is used in the endcaps. High voltage is supplied by a CAEN HV supply for each endcap. Each Dee is split into two quadrants, and a 800 V line and a 600 V line are supplied from the CAEN supply to each quadrant. From there, the lines fan out to give each supercrystal one 800 V and one 600 V line. A second fanout, provided by high voltage filter cards in each supercrystal, then supplies each individual VPT with one 800 V and one 600 V line for the anode and dynode respectively.

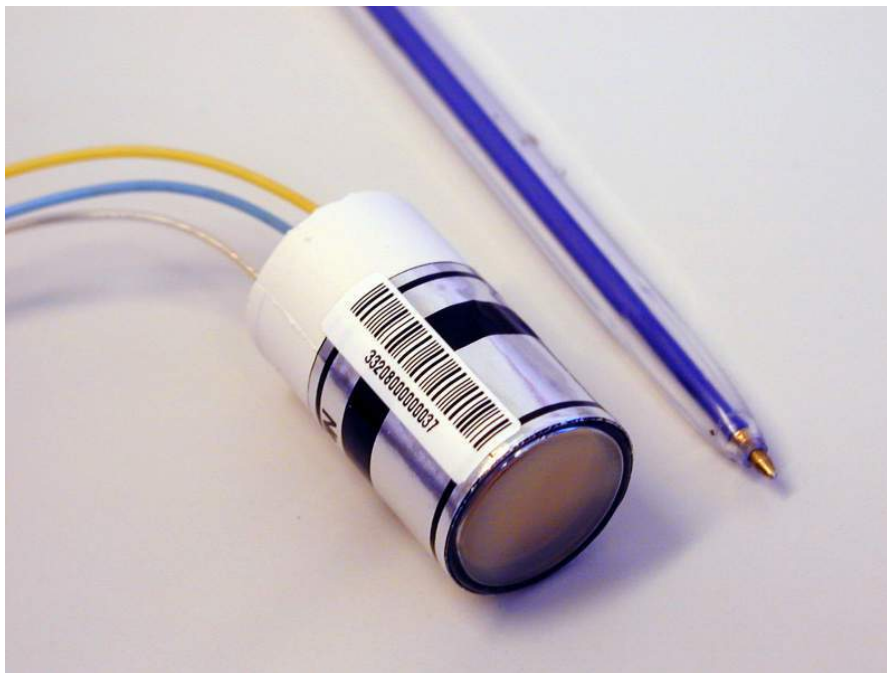


Figure 3.8: An example of a VPT used in the endcaps of the CMS ECAL.

3.4 Laser Monitoring System

Since the response of each individual crystal and VPT varies over time, a laser monitoring system has been introduced to measure and correct for the changes.

Laser light pulses are injected into the crystals using an optical fibre distribution system. This delivers pulses to the selected calorimeter region for the endcaps. A two level fanout delivers pulses to each individual crystal, as well as to a reference PN photodiode. The laser light is delivered to the rear face of each crystal by a quartz fibre optic cable. This light then propagates to the front of the crystal and is internally reflected to the rear of the crystal where it is detected by the VPT. The reference photodiode is used to calibrate the level of the injected light [12].

The crystals in a particular calorimeter region are pulsed every 40 minutes. The pulses are 88.924 μs apart. The wavelength of light used in 2011 was 440 nm and in 2012 was 447 nm. Monitoring is continued after LHC fills to track the recovery of each channel. This monitoring allows measurements of the response of each combined crystal and VPT to be made, and for these to be calibrated correctly [12].

The degradation and recovery of the response of both the VPTs and crystals is shown in Figure 3.10. The bottom plot in Figure 3.10 shows the start-of-fill instantaneous LHC luminosity that increased from approximately $1 * 10^{33} \text{cm}^{-2} \text{s}^{-1}$ at the start of 2011 to almost $8 * 10^{33} \text{cm}^{-2} \text{s}^{-1}$ at the end of 2012. The higher luminosity results in higher radiation levels so the crystals and VPTs experience more damage and their response drops. At the very highest value of η , above 2.7, the EE response at the end of 2012 is approximately just 30% of that at the start of 2011. This represents the highest irradiated region. The outer EE region for η from 1.5 to 1.8 has a response at the end of 2012 which is 90% of that at the start of 2011.

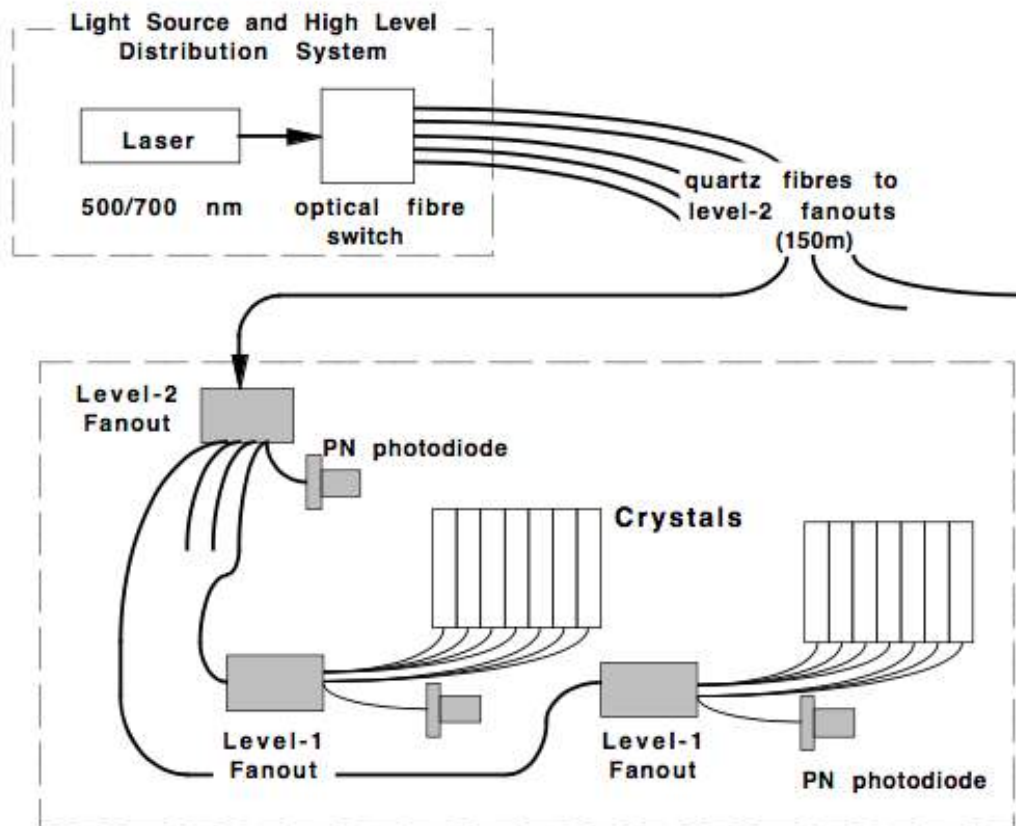


Figure 3.9: ECAL laser monitoring system. The light source and high-level distribution system feed into a two-level distribution system to supply light to each crystal in the ECAL [12].

3.5 LED Pulsar System

A Light Emitting Diode (LED) pulser system has been introduced in the endcaps and is complementary to the laser system. It has a dual purpose which is to stabilise the VPTs in the EE and to assist the laser system in measuring the response of the detector. It delivers pulses with a wavelength of 455 nm at a rate of 100 Hz with approximately 50 GeV equivalent energy to all of the VPTs. These pulses ensure that the VPTs are kept active even in the absence of LHC collisions.

The LEDs are driven by high output current op-amps. The drive pulses have an amplitude of 1.2 A and a width of 80 ns. The light sources and drive circuits are housed in four metal enclosures which are mounted on the circumference of each Dee.

The schematics for the LED system are shown in Figure 3.11. An optical fibre is inserted to the lens of each LED. The fibres from the LEDs are grouped and transport the light to a diffusing sphere. The light from the laser monitoring system is delivered to the same diffusing sphere. This light is then distributed to approximately 250 channels through individual optical fibres. The light from the LEDs enters the rear face of each crystal through the same fibres as the laser system. The LED light is internally reflected from the front face to reach the VPT. This system is synchronised to pulse during the 3 μ s abort gaps which occur during each 89 μ s cycle of the LHC beams [11].

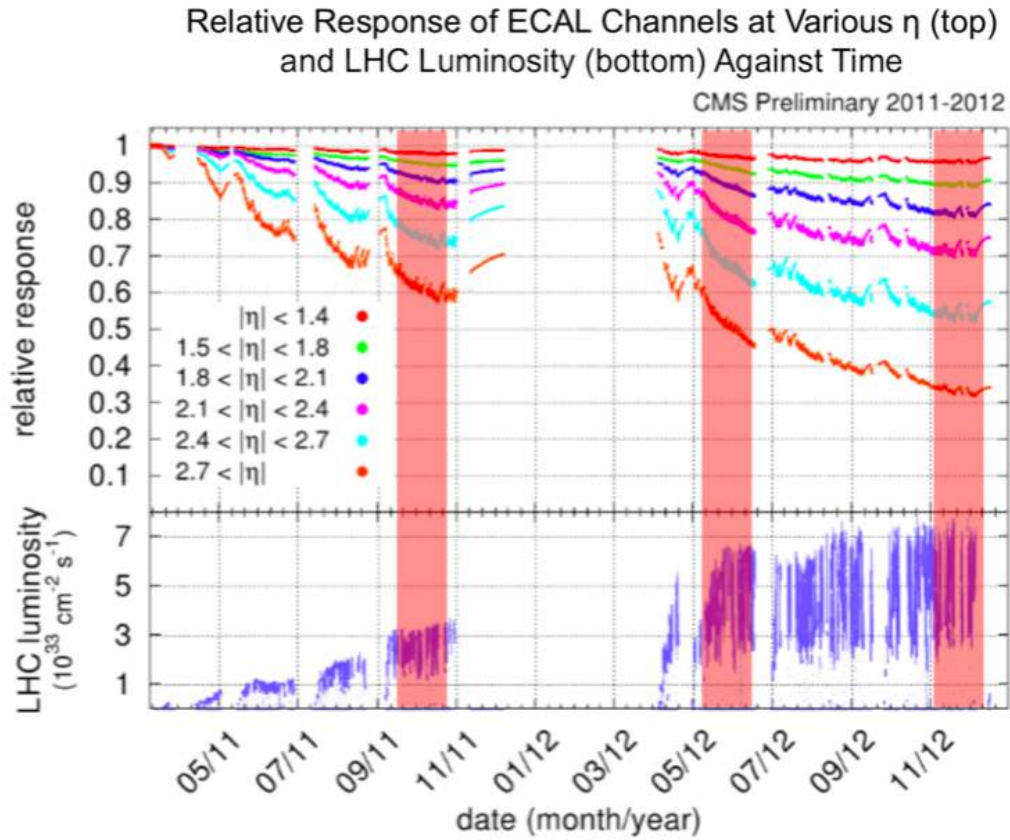


Figure 3.10: The laser response history of the ECAL in 2011 and 2012. The top graph shows the average relative response, normalised to the beginning of operation in 2011, for crystal/VPT channels in particular bands of pseudorapidity. The bottom plot shows the instantaneous LHC luminosity over the same time period [18]. The three shaded areas are October 2011, May 2012 and December 2012 which were the three time periods used in this project.

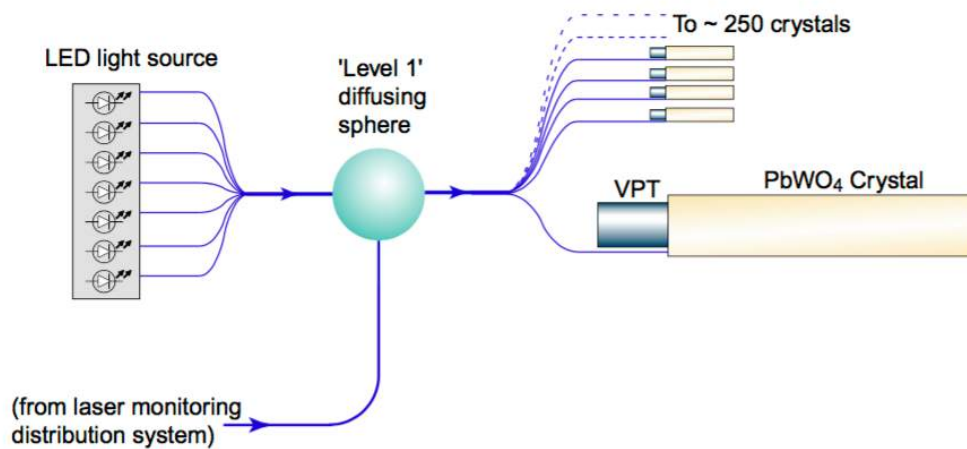


Figure 3.11: Schematic diagram showing the distribution system for the ECAL LED pulser system [11].

4

The Study of VPT Instabilities

The two key areas for investigation were the stability of the VPTs in the endcap and the effectiveness of the LED pulser system in stabilising them. A summary of the results from previous studies is included below.

In 2008, a month long light load simulation of the LHC was undertaken to test the response of 200 production VPTs within CMS, both with and without the CMS 3.8 T magnetic field. LED light pulses were provided at 10 kHz for 17 hours at a time to simulate a typical cycle of LHC operation. Without the magnetic field, the tests reported a 4-5% change in the average response of the VPTs when the light load was removed. However, in the presence of the 3.8 T field the average response only changed by 0.1% when the load was removed. This demonstrates that the 3.8 T field considerably improves the stability of the VPTs. These results are shown in Figure 4.1 [19].

A second simulation in 2010 at the University of Virginia investigated the effect of the LED pulsers on the stability of the VPTs. Five VPTs were put under simulated LHC conditions for 16 hours on, 8 hours off cycles [8]. The VPTs in the LHC simulation were in a 3.8 T magnetic field and a luminosity equivalent of $10^{34} \text{ cm}^{-2} \text{ s}^{-1}$.

The LHC was simulated with a special set of LEDs pulsing at 10 or 20 kHz (the load light) to give 1-10 nA from the photocathode. The stability pulser (soak light) was run at 100 Hz with separate LEDs and the VPT responses were taken from the soak light pulse size.

Figure 4.2 shows the largest of the effects seen for the VPTs tested. It shows that the step in response at the end of a fill is reduced from 1.7% without the 100 Hz stability pulses to 0.7% with the 100 Hz pulsing. Overall, similar effects could be seen for two of the four VPTs. A 1.7% step in response would damage the ECAL target of 0.5% energy resolution for photon and electron measurements, so a reduction of 1% in step size is encouraging.

The work on the steps in response concerned photocathode currents of 1-10 nA. The effect of the magnetic field, in Figure 4.1, was carried out with photocathode currents of only 0.1 nA. An important part of this project was to investigate if there is a correlation between step size and the photocathode current drawn from the VPTs.

The analyses mentioned in this section involved pulsed light simulations of the LHC load. In this report real data from proton-proton fills at the LHC itself will be used to further investigate and quantify the

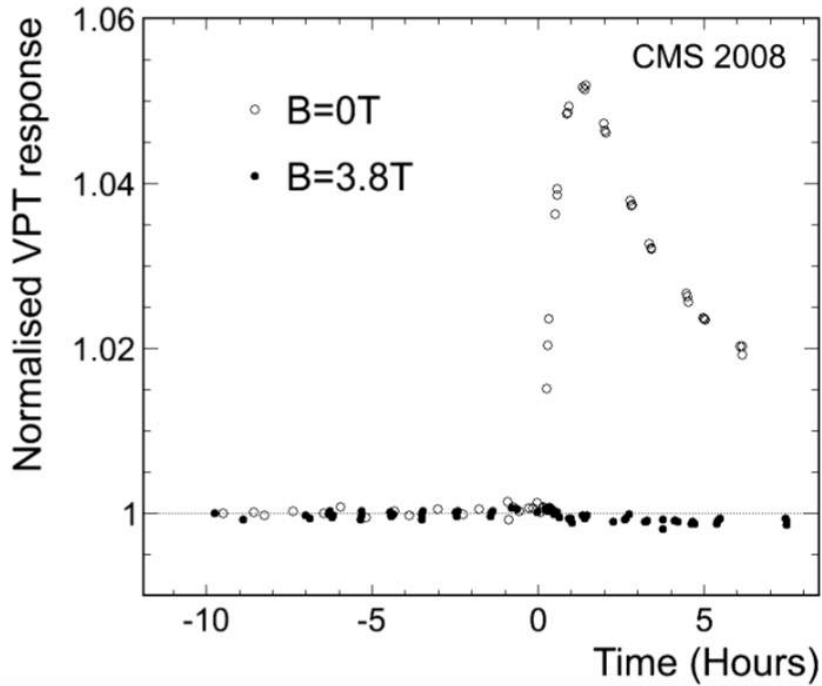


Figure 4.1: Average normalised response of 200 production VPTs for an LHC simulation at 0 T (open circles) and 3.8 T (filled circles). A pulse load of 10 kHz was supplied for 17 hours and turned off at $T=0$ hours. The VPT response was normalised to $T=-10$ hours [19].

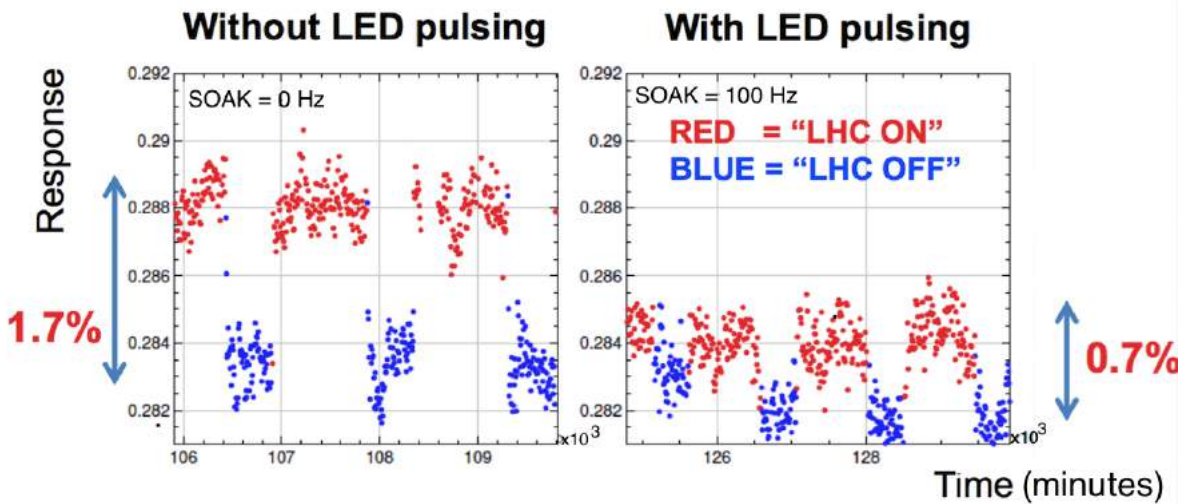


Figure 4.2: Laboratory measurement of the response of CMS VPT 2181 against time for simulated LHC on/off cycles with soak light at 0 Hz (left) and 100 Hz (right). Red points represent LHC on and blue LHC off.

VPT steps.

5

VPT Photocathode Currents

The light load experienced by a VPT towards the end of an LHC might determine the step in response of the VPT at the end of a fill. Therefore, for this analysis, it was important to estimate the loads experienced by the VPTs. The VPT photocathode current represents this load. The photocathode currents are derived from the anode currents supplied by the CAEN HV supplies and take into account the VPT positioning across the EE and the luminosity for the fill. The photocathode currents for each VPT in EE+, at the end of each fill, can be estimated. This section explains how these estimates are made.

5.1 CAEN Anode Currents

The measured CAEN anode current for each quadrant in EE+ at any time can be accessed from the CMS web-based monitoring system (CMSWBM). The measurements update after a change of at least $0.5 \mu\text{A}$, and are held at a baseline between 365 and $366 \mu\text{A}$ depending on the quadrant.

Figure 5.1 shows an example of these HV current measurements for one quadrant for a fill on 16th October 2011 to 17th October 2011. The maximum value it reaches is $369 \mu\text{A}$, which corresponds to an actual current of $3 \mu\text{A}$ when the baseline is taken into account.

5.2 Estimating VPT Photocathode Currents

For the purpose of these estimates, the anode currents taken from CMSWBM for the four quadrants in EE+ are summed together to give a total anode current, I_{tot} , for EE+. The total anode current is used to extract photocathode currents using equation 5.1.

$$I_{tot} = A \sum_{allEE+} R * G_{corr} * QE * L \quad (5.1)$$

where A is a constant to be determined.

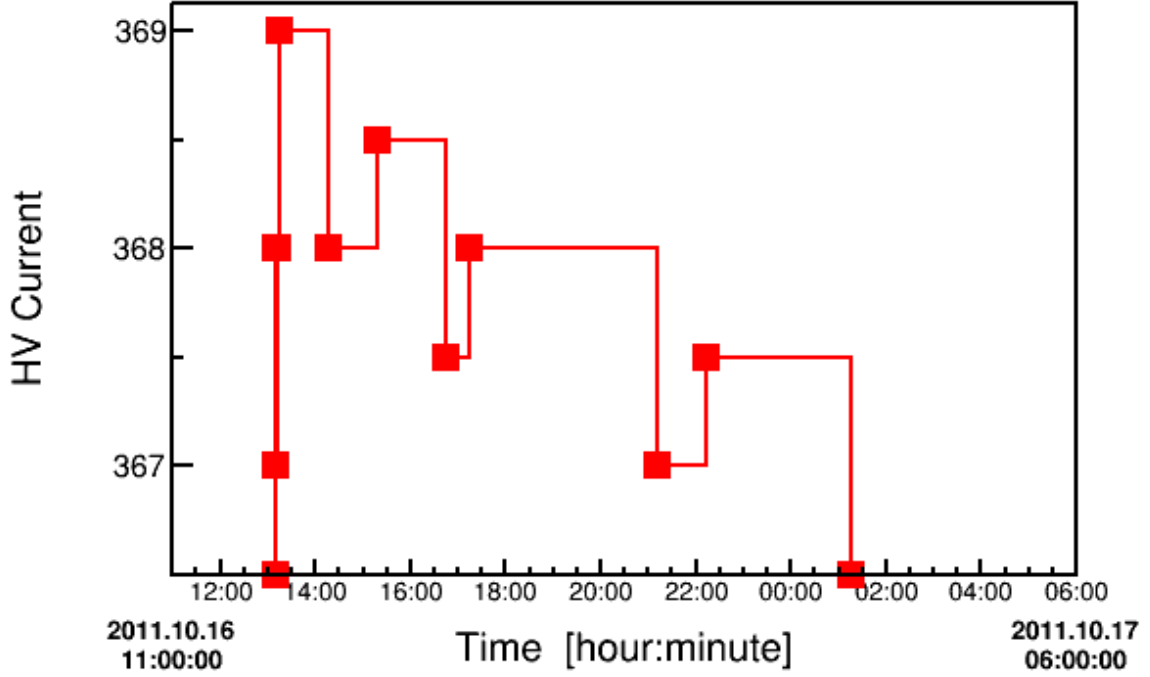


Figure 5.1: CAEN HV current measurements from CMSWBM for Dee 1 Ch 2 on 16th-17th October 2011. The HV current is in units of μA .

R is the relative radiation value for the VPT. It is the deposited energy in the volume of a lead tungstate crystal at a luminosity of $10^{34} \text{ cm}^{-2} \text{ s}^{-1}$ which has been determined for specific pseudorapidities using dose maps from Monte Carlo simulations.

G_{corr} is the corrected response for the VPT. The response for each VPT was measured during ECAL construction at magnetic field $B=0 \text{ T}$ and anode/dynode high voltage supply $HV = 1000/800 \text{ V}$. Response corrections have been applied for $B=3.8 \text{ T}$ and $HV=800/600 \text{ V}$ used in the endcaps [20].

QE is the quantum efficiency which was also measured during ECAL construction for each VPT.

L represents the response loss of the channel, due to crystal darkening and VPT response loss. It is the fraction of the channel's response during the fill compared to the response at the start of operation in 2011.

The constant A can then be found and is given by

$$A = \frac{I_{tot}}{\sum_{allEE+} R * G_{corr} * QE * L} \quad (5.2)$$

The anode current for a single VPT can then be determined.

$$i_{anode} = A * R * QE * G_{corr} * L \quad (5.3)$$

The VPT photocathode current is estimated by dividing the anode current by G_{corr} .

$$i_{cathode} = A * R * QE * L \quad (5.4)$$

6

LHC Data For Analysis

To compare the stability of pulsed and unpulsed VPTs, a time period with both pulsed and unpulsed regions in the endcap was used. In October 2011 and December 2012, 6539 of the 7324 VPTs in EE+ were pulsed and 785 unpulsed, as shown in Figure 6.1. The instantaneous LHC luminosity at the end of fills ranged from $1.5 * 10^{33} \text{ cm}^{-2} \text{ s}^{-1}$ to $3 * 10^{33} \text{ cm}^{-2} \text{ s}^{-1}$ in October 2011 and from $2.5 * 10^{33} \text{ cm}^{-2} \text{ s}^{-1}$ to $5.2 * 10^{33} \text{ cm}^{-2} \text{ s}^{-1}$ in December 2012, as shown in Figures 6.2 and 6.3. This factor of ~ 3 in instantaneous luminosities allows for a comparison between different LHC conditions and could provide predictions for the VPT stability for LHC luminosity increases in 2016 and beyond.

Figure 3.10 in section 3.4 shows that, for the highest pseudorapidity regions ($\eta > 2.7$), the average normalised response of the crystals and VPTs fell from roughly 0.6 in October 2011 to 0.35 in December 2012. This factor of 1.7 decrease in the response is due to roughly equal reductions in crystal transparency to scintillation light and a reduction in VPT photocathode efficiency. The resulting VPT photocathode currents are therefore similar despite the different luminosities in these two time periods. To investigate conditions with different VPT photocathode currents, a time period where the luminosities and responses combine to give higher photocathode currents was also needed. The time period chosen was in May 2012. The response levels are similar to that of October 2011 but the final LHC luminosities are higher, as shown in Figure 6.4, which results in higher VPT photocathode currents.

Data from the laser monitoring system has been used to track the response of each channel in EE+ in the mentioned time periods.

6.1 Comparison Between Steps at the Beginning and End of Fills

Figure 1.6 in section 1 shows an example of a step in response at the beginning and end of an LHC fill. At the beginning of the LHC fill the response of the channel drops from approximately 0.573 to 0.555. At the end of the fill, the response jumps from approximately 0.555 to 0.560 at the next measured point.

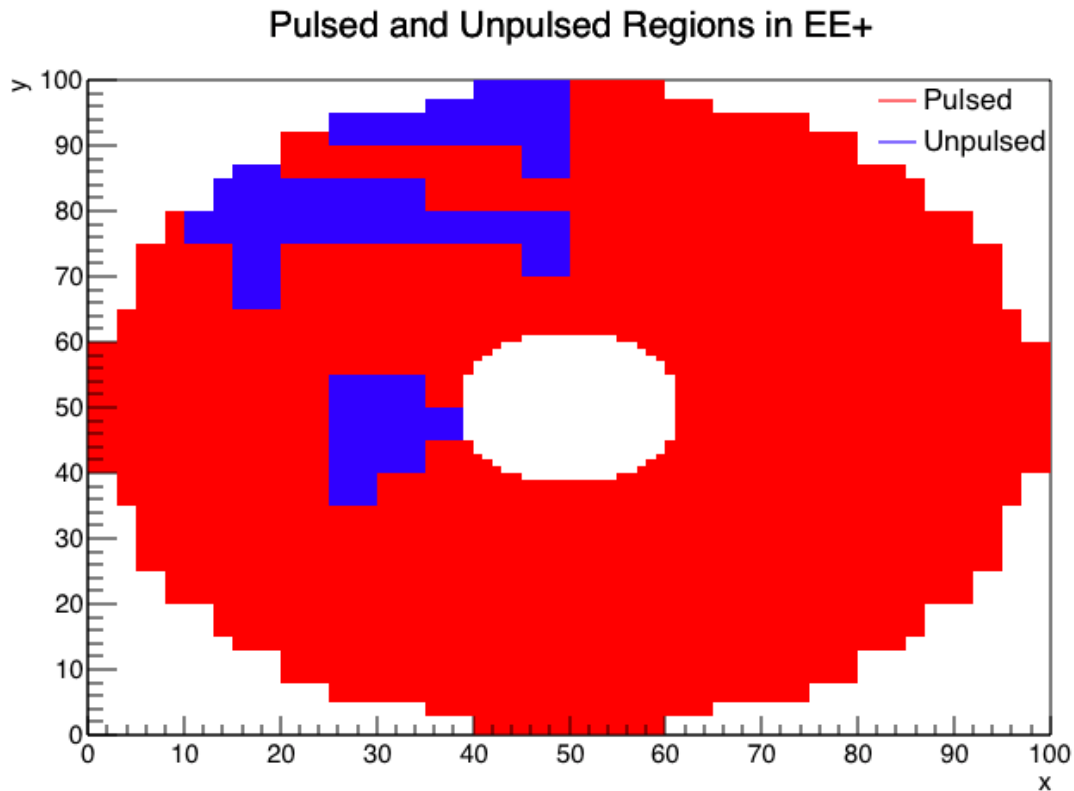


Figure 6.1: Pulsed and unpulsed regions of EE+ in October 2011 and December 2012 (Red is pulsed, blue is unpulsed). The pulsed regions comprise 6539 crystals and the unpulsed regions comprise 785.

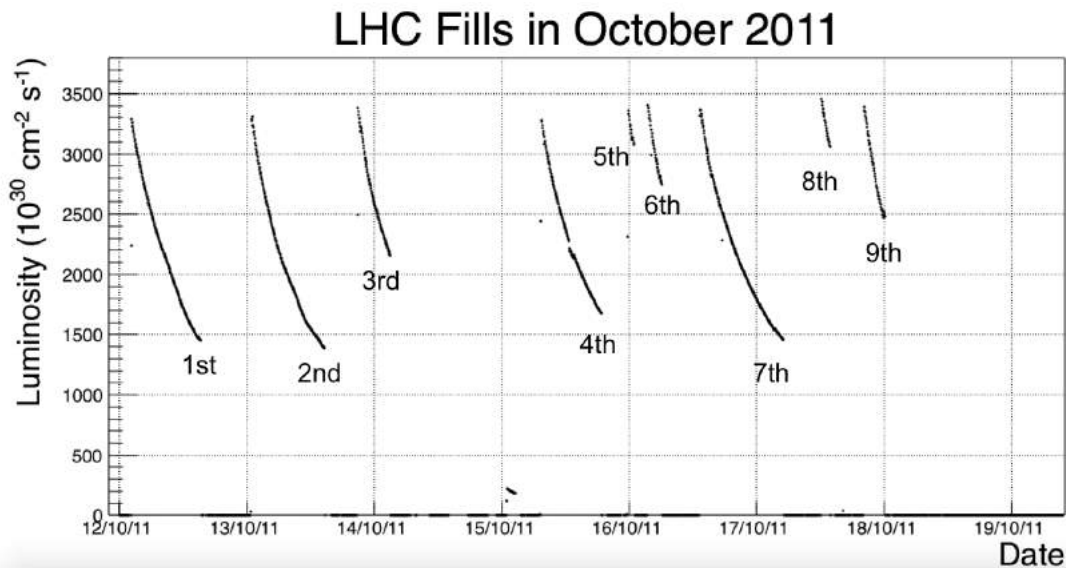


Figure 6.2: Instantaneous luminosities ($10^{30} \text{ cm}^{-2} \text{ s}^{-1}$) against date for the LHC fills in October 2011

The step at the beginning of the fill is more than three times larger than at the end of the fill. However, the step at the beginning is more complex and difficult to evaluate because it involves response losses due to both crystal radiation damage and the VPT steps. The step at the end of the LHC fill is assumed

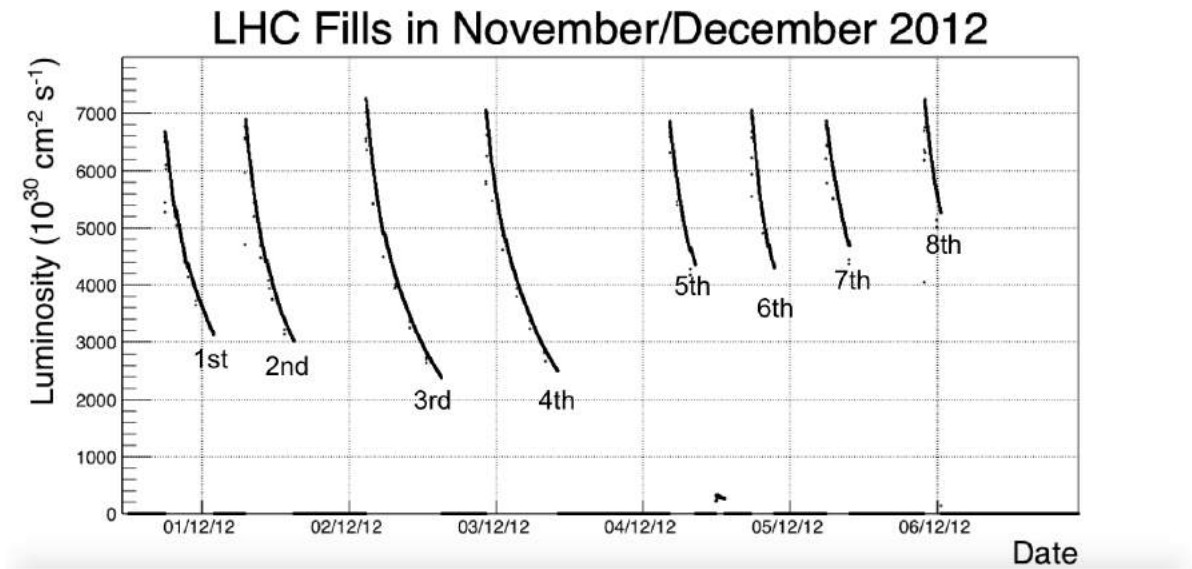


Figure 6.3: Instantaneous luminosities ($10^{30} \text{ cm}^{-2} \text{ s}^{-1}$) against date for the LHC fills in December 2012

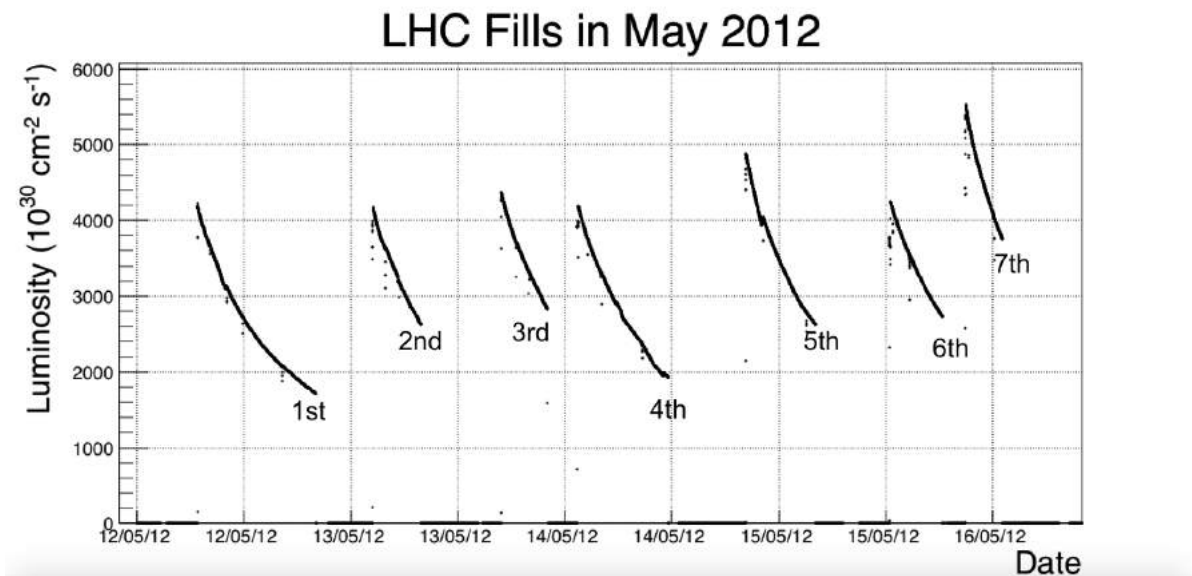


Figure 6.4: Instantaneous luminosities ($10^{30} \text{ cm}^{-2} \text{ s}^{-1}$) against date for the LHC fills in May 2012.

to be mainly attributable to a rapid change in only the VPT response, and is therefore the 'step' which will be used in this report.

6.2 Estimating Step Size

The laser monitoring system takes measurements every 40 minutes. An estimate of the step size, for each VPT at the end of each fill, uses laser monitoring data close to the step. The response just before and just after the fill is estimated from the time periods before and after the fills where there is a near linear correlation between response and time. A fit is made to the data leading up to the end of the fill. This is used to determine the response at the end of the fill. A separate fit is made to the data after

the fill to provide the response at the start of the no fill period. The step size response is the difference between these two values. Figure 6.5 shows examples of these fits. This procedure was carried out for all the channels in EE+.

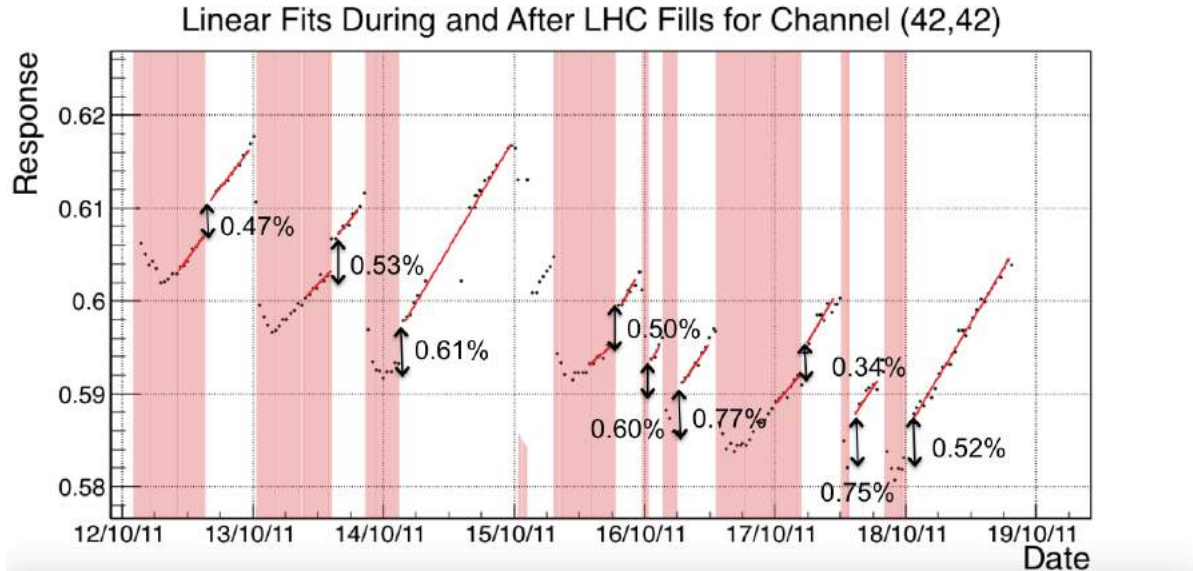


Figure 6.5: Response of channel (41,41) normalised to the beginning of 2011, against date. The shaded red areas show the periods of LHC fills with collisions. The white regions are periods where the LHC is off.

In Figure 6.5, some fills are too short for any kind of reliable fit. Instead the closest measured value to the end of the fill is used. This was also the case for a number of fills in May 2012 and December 2012. The fills where this method has been used instead of the fits are listed in Table 6.1.

October 2011		May 2012		December 2012	
Fill Number	Date	Fill Number	Date	Fill Number	Date
3rd	14/10/2011	2nd	13/05/2012	6th	04/12/2012
5th	16/10/2011	3rd	13/05/2012	7th	05/12/2012
6th	16/10/2011	7th	15/05/2012	8th	06/12/2012
8th	17/10/2011				
9th	18/10/2011				

Table 6.1: Fills where the last measured values is used instead of a fit.

The fill on 15/05/2012 (6th fill in the May 2012 set) was not used in this analysis because no reliable measurements of response were made by the laser monitoring system after the end of this fill. The fill on 04/12/2012 (5th fill in the December 2012 set) was not used due to luminosity discontinuities.

The step size was calculated for every VPT in EE+, for every valid fill in the three time periods. This report primarily presents the results from October 2011, but also discusses similarities and differences with the May and December 2012 data.

Two calculations of the step size are used in this report, a relative step size and an absolute step size. The response of each channel is normalised to the response at the beginning of 2011. The relative step size as a percentage of the response at a particular time is useful for looking at the possible effect on resolution for physics. For example, a relative step size of 2% would result in an error of 2% in measurements taken in this time period. The absolute step size with respect to the start of 2011 is more useful when trying to understand the internal workings of the crystals and VPTs.

7

Step Size and VPT Position

VPTs across EE+ receive different radiation levels which are dependent on their position in the endcap. Towards the centre of the endcap, at higher η , the radiation levels are higher which results in a higher load on the VPTs. Consequently, at the end of an LHC fill the change in load experienced by these VPTs was expected to be larger, resulting in larger steps in the VPT response towards the centre of the endcap.

The size of the VPT steps may be dependant on LHC luminosity. As a consequence only the plot for the first fill in 2011 is shown. Any similarities or differences with the other fills are discussed.

Figure 7.1 shows the average percentage step size as a function of η for the first fill considered in 2011. The percentage steps are smaller than seen in laboratory data. The largest step is $0.7\% \pm 0.09\%$ at $\eta \simeq 2.8$. Most of the steps are under 0.5% which is the CMS ECAL target resolution for electron and photon measurements. Laboratory data showed steps of 1.7% for an unpulsed VPT and 0.7% for a pulsed VPT.

Figure 7.1 shows that percentage step size increases approximately linearly towards higher η , as expected. The results from the other fills in 2011 have the same correlation. Below an η value of 2.8, the pulsed and unpulsed VPTs appear to follow the same relationship. There is slightly more variation in the steps of unpulsed VPTs but this may be attributable to the much smaller sample of unpulsed VPTs available for this analysis (6539 pulsed and 785 unpulsed). Above $\eta=2.8$, the unpulsed VPTs experience percentage steps between 0.12 and 0.22 larger than the pulsed VPTs. However, there are only eight or fewer VPTs in this region. Consequently, these unpulsed results are not considered sufficiently statistically accurate at this stage.

The May 2012 percentage step size against η have a similar positive linear relationship between percentage step size and η . The step size peaks at $0.95\% \pm 0.1\%$ for the seventh fill. This may be due to the increased LHC luminosity resulting in higher VPT photocathode currents and increased loads on the VPTs. All VPTs in May 2012 were unpulsed so they provide no further information on the efficacy of the LED pulsers.

Figure 7.2 shows the percentage step size against η in December 2012. All the fills in December 2012 followed the same general shape. The step size of the pulsed VPTs increases approximately linearly with η , up to $\eta=2.3$, and peak at 0.65%. Beyond $\eta=2.3$ the step size decreases linearly down to less

than 0.4% at $\eta=2.9$.

The drop in percentage step size in December 2012 at high η was unexpected. It is even more evident when looking at the absolute step size instead of percentage step size, as shown in Figure 7.3. To confirm that these unexpected results are correct and that this is not due to an error in step size estimates, the laser data of a number of channels were checked individually. An example is shown in Figure 7.4. The data are consistent with those in Figure 7.2.

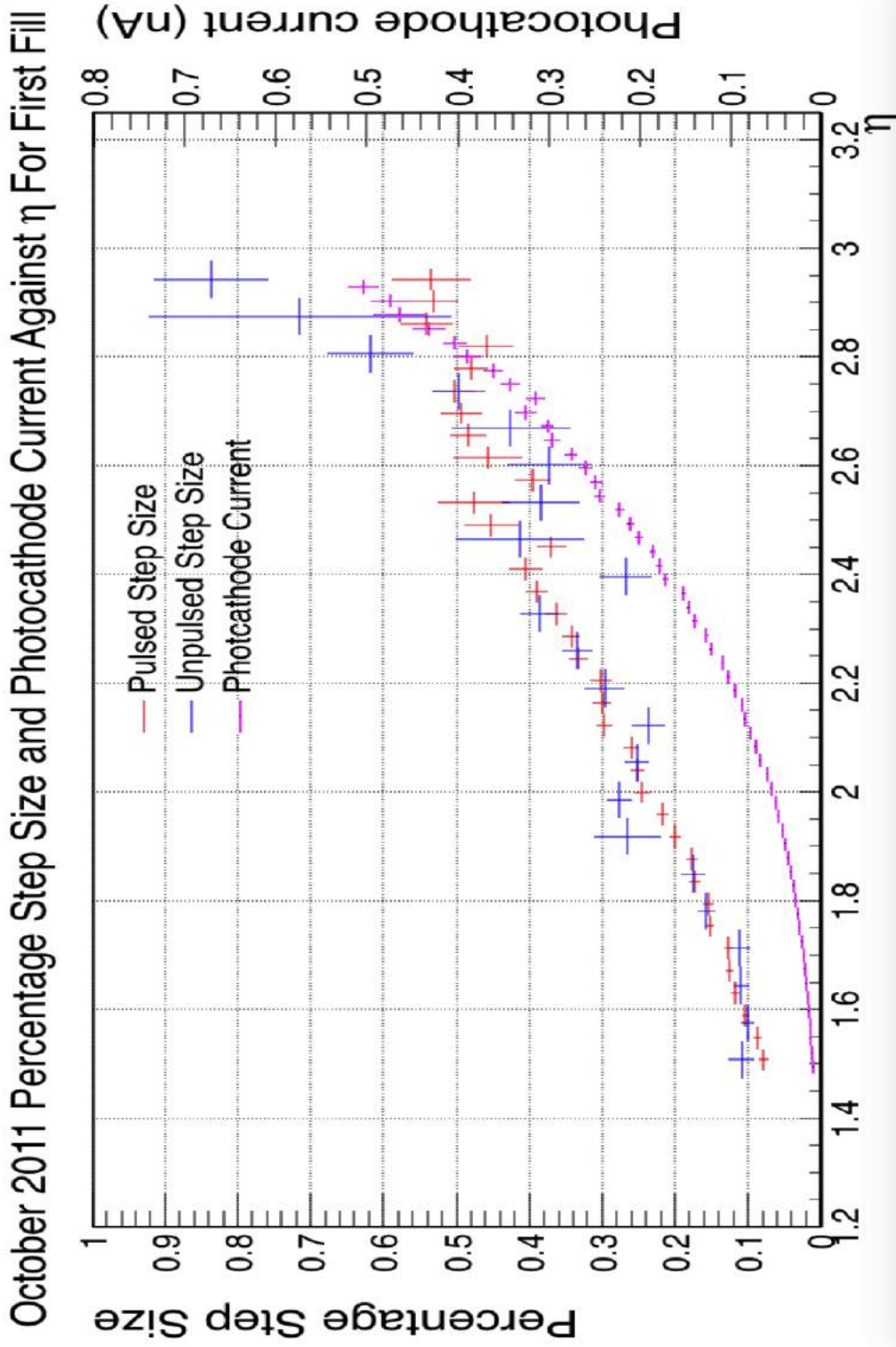


Figure 7.1: The average step size for pulsed (red) and unpulsed (blue) VPTs and the VPT photocathode current (magenta) at the end of the first fill in the October 2011 set against η . The final LHC luminosity was approximately $1.5 \times 10^{33} \text{ cm}^{-2} \text{ s}^{-1}$. The left-hand vertical axis shows the VPT step size as a percentage of the VPT response at the end of the fill. The right-hand vertical axis shows VPT photocathode current in nA.

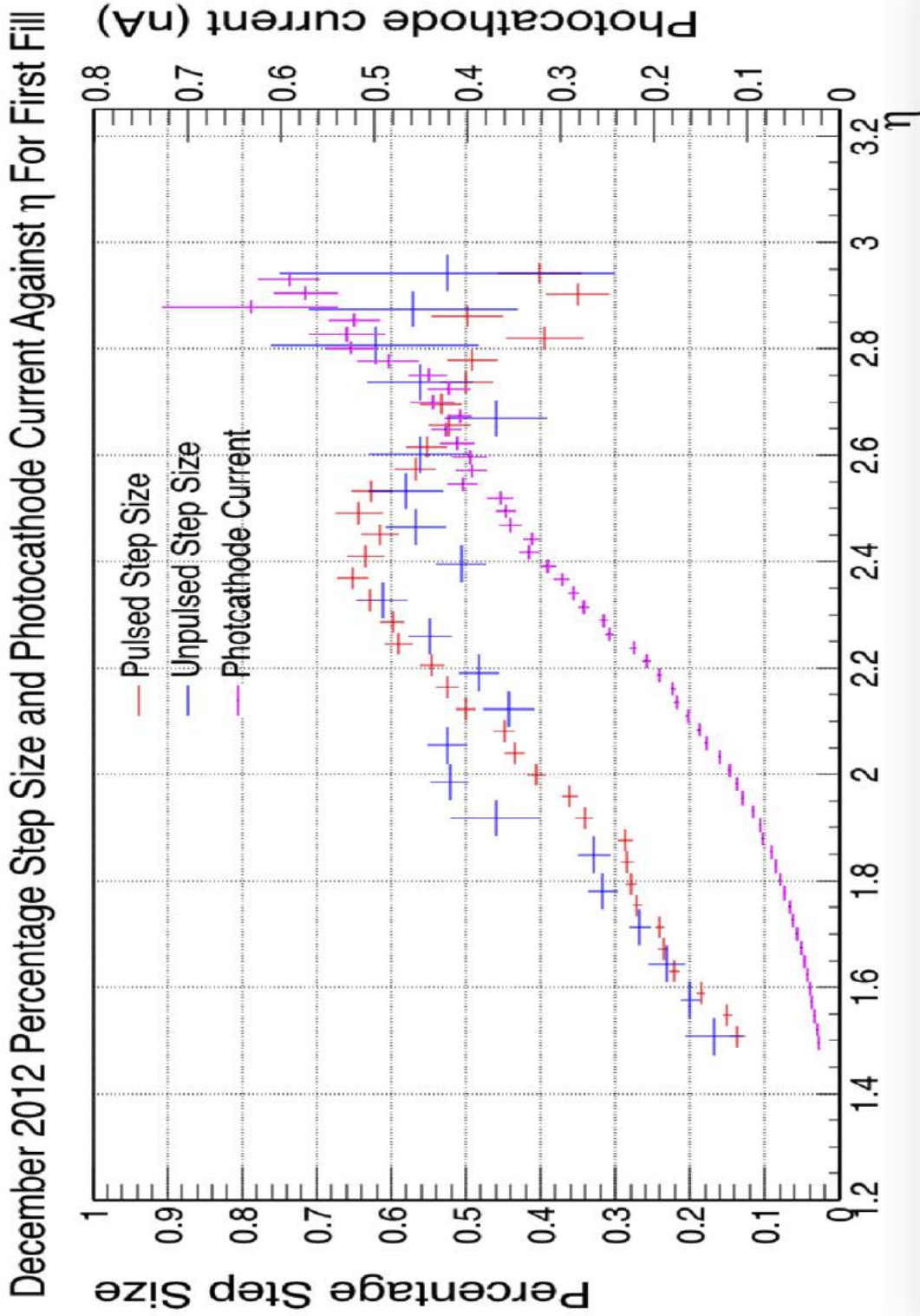


Figure 7.2: The average step size for pulsed (red) and unpulsed (blue) VPTs and the VPT photocathode current (magenta) at the end of the first fill in the December 2012 set against η . The final LHC luminosity was approximately $3 \times 10^{33} \text{ cm}^{-2} \text{ s}^{-1}$. The left-hand vertical axis shows the VPT step size as a percentage of the VPT response at the end of the fill. The right-hand vertical axis shows VPT photocathode current in nA.

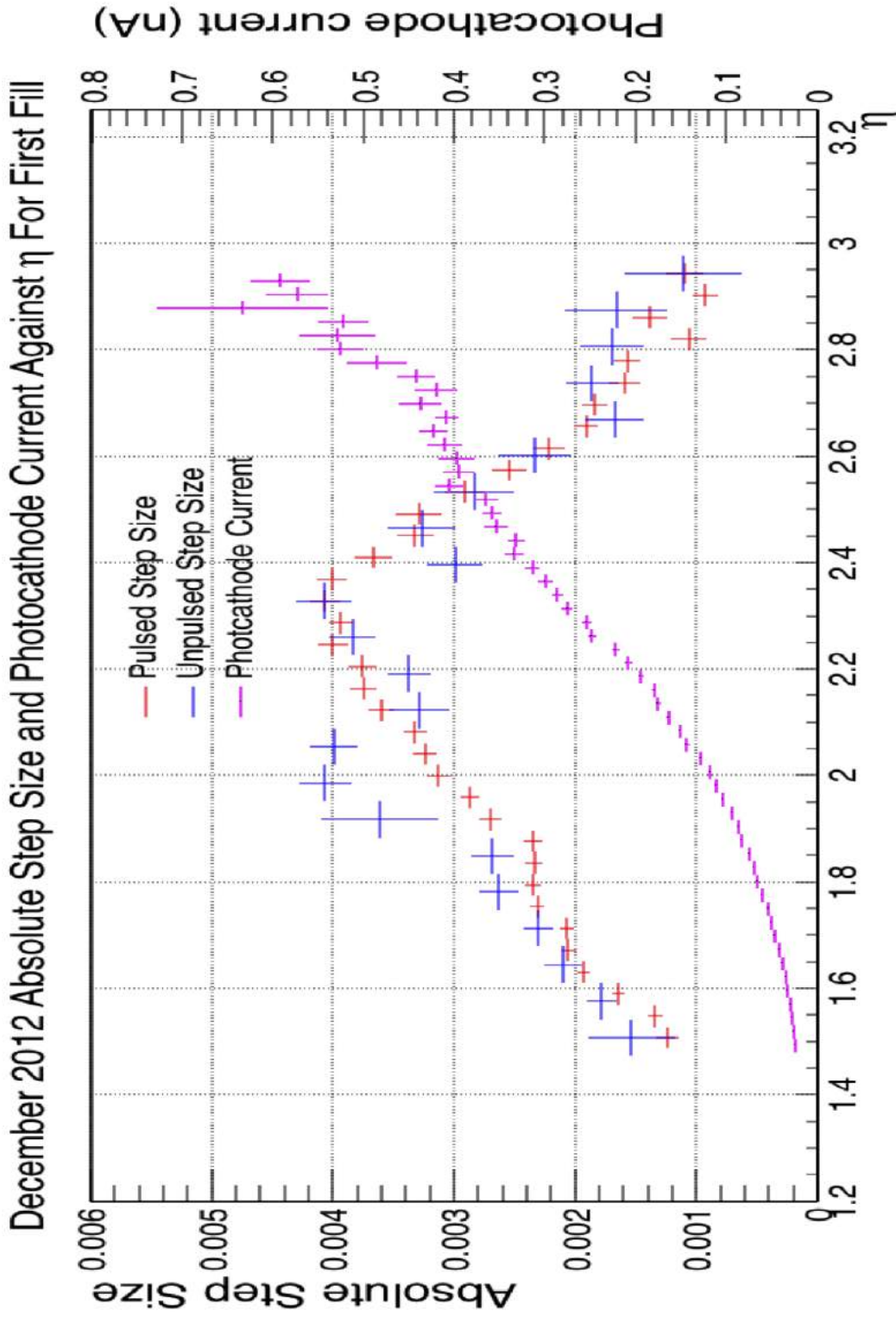


Figure 7.3: The average absolute step size for pulsed (red) and unpulsed (blue) VPTs, and the VPT photocathode current (magenta), at the end of the first fill in the December 2012 set against η . The end-of-fill LHC luminosity was approximately $3 \times 10^{33} \text{ cm}^{-2} \text{ s}^{-1}$. The left-hand vertical axis shows the absolute VPT step size, where the VPT response has been normalised to the beginning of 2011. The right-hand vertical axis shows the VPT photocathode current at the end of the fill.

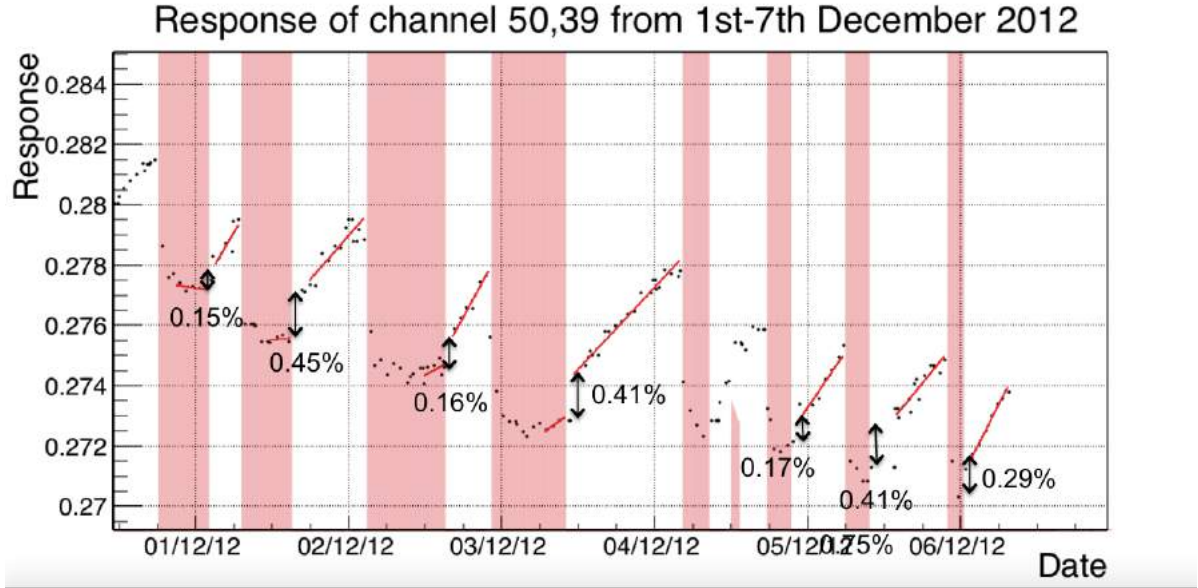


Figure 7.4: Response of channel (50,39) normalised to the beginning of 2011, against date. Shaded red areas are LHC on and white are LHC off. Red lines show the linear fit to the data towards the end of each fill. The end of fill percentage step sizes vary from 0.15% to 0.45%.

There were two main differences between the fills in December 2012, and the fills in October 2011 and May 2012. December 2012 had end-of-fill LHC luminosities roughly double that of October 2011 and 1.5 times that of May 2012: The second difference relates to the degradation in response of the VPTs and crystals. The average response, normalised to the beginning of 2011, in these high η regions was approximately 0.35, 0.5, and 0.6 for December 2012, May 2012 and October 2011 respectively. However, as Figure 7.3 shows, these factors still resulted in increasing photocathode current for increasing η , even in December 2012. This increased load was expected to increase the step size. It is unclear why this reduction in step size happens beyond $\eta=2.3$.

There are two sets of crystals, from different manufacturers, in the EE. The point in Figure 7.3, for December 2012, where step sizes begin to fall is at approximately $\eta=2.35$, where the crystal producer changes. Russian (BTCF) crystals are used for $\eta < 2.35$. Chinese (SIC) crystals are used for $\eta > 2.35$. It is possible that these steps are not due solely to changes in VPT response and that changes in crystal transparency are also involved. If this is the case then steps would also be seen in the ECAL barrel where VPTs are not used. This can be investigated in the future.

In terms of the effect on physics results, these results are promising. Although the LED pulsers do not appear to lessen the magnitude of the VPT steps in these fills, the average VPT steps are all under 1%, with the vast majority below the CMS ECAL 0.5% precision target. The steps are much smaller than the 1.7% steps seen in laboratory tests. While unexpected and unexplained, the fact that step size decreases at high η in December 2012 is a good result. Future LHC conditions will tend to higher LHC luminosities and more of the endcap will experience the conditions that the inner region experienced in December 2012.

8

Step Size and Instantaneous LHC Luminosity

The anode currents within EE+ correlate closely with LHC luminosity, as shown in Figure 8.1. The VPT photocathode current is proportional to anode current so a higher LHC luminosity results in higher VPT photocathode currents. The VPT photocathode current represents the load on the VPT. A larger LHC luminosity, and consequently larger load on the VPT, was expected to cause larger VPT response steps.

Figure 8.2 shows the percentage step size against luminosity for VPTs at a radius of 0.3-0.41 m for the three time periods. The step size is essentially independent of the instantaneous luminosity. This is possibly due to the fact that luminosity is not the only factor affecting VPT load. In this central region, with high radiation levels, the highest average percentage step size is 0.9 ± 0.15 . This result is from the unpulsed VPTs in May 2012. The steps are much smaller than the 1.7% seen in the laboratory. The steps followed a linear relationship with η in May 2012, so the majority of VPT steps were much lower than $0.9\% \pm 0.15\%$ and closer to the 0.5% resolution target for the ECAL.

Figure 8.3 shows step size against luminosity for pulsed and unpulsed VPTs in October 2011 towards the centre of EE+. It is consistent with Figures 7.1 and 7.2 in section 7. The central VPTs at high η experience a slightly larger step size if they are unpulsed than if they are pulsed. The difference is roughly 0.1% on average. The December 2012 results agreed with this.

Figure 8.4 shows the same plot for May 2012. All VPTs in this period were unpulsed. However, the VPTs that were pulsed and unpulsed in October 2011 and December 2012 are still shown separately in the plot, in red and blue respectively. The same difference in step size between the two groups is still seen, even though all VPTs were unpulsed. It appears that this group of VPTs, at the centre of EE+, that were unpulsed in October 2011 and December 2012, naturally experience larger steps in response and that the LED pulsing had no effect.

Percentage step sizes have been used in this report for looking for correlations with luminosity. The absolute step size also shows no correlation with luminosity.

Luminosity and Anode Current for Dee 1, Channel 2 from CMSWBM

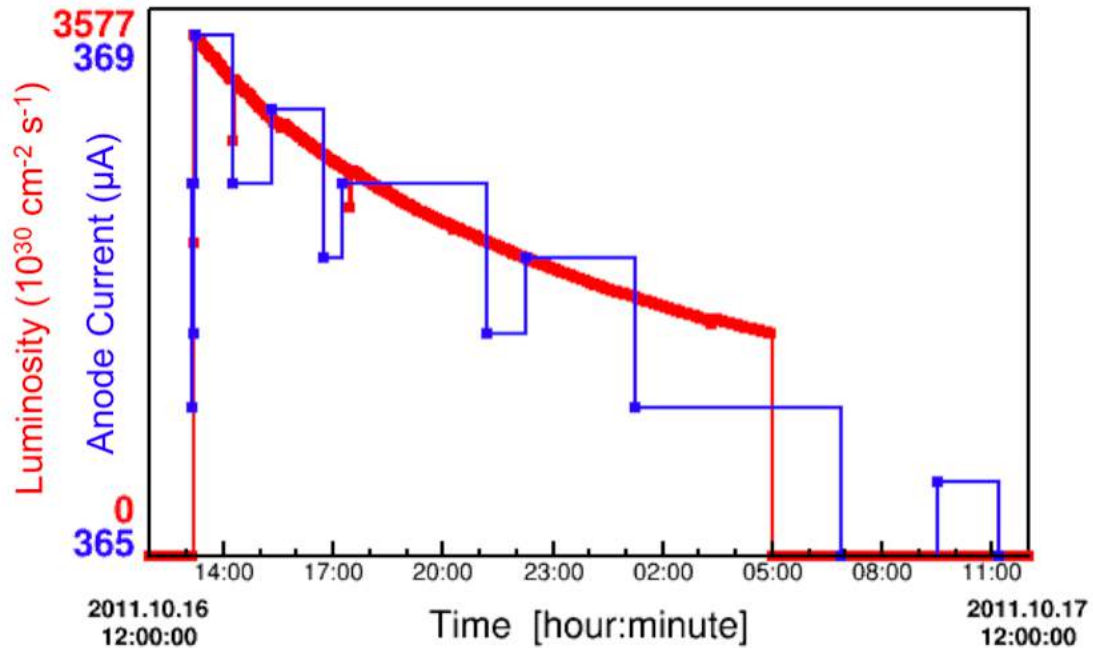


Figure 8.1: The LHC instantaneous luminosity (displayed in units of $10^{30} \text{ cm}^{-2} \text{ s}^{-1}$) in red, and anode current (μA) in blue, against time for 16-17th October 2011. The anode current shown is for Dee 1, channel 2 of EE+. The current has a baseline of $365.5 \mu\text{A}$. The measurement precision is $0.5 \mu\text{A}$. The system updates after a change larger than $0.5 \mu\text{A}$.

Percentage Step Size Against End Luminosity for Pulsed VPTs Within Radius 0.31-0.40m

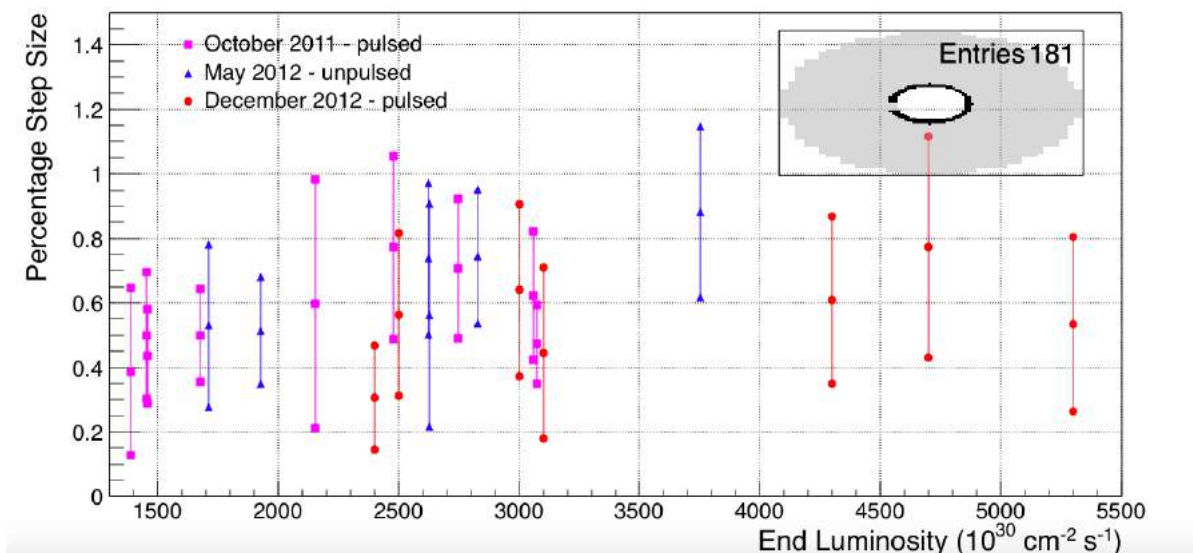


Figure 8.2: Mean and RMS of step size against luminosity ($10^{30} \text{ cm}^{-2} \text{ s}^{-1}$) for radius 0.31-0.40 m. Step size is as a percentage of response at end of fill. Magenta square, blue triangular and red circular points correspond to October 2011, May 2012 and December 2012 respectively. Inset graph shows which VPTs were used in black.

October 2011 Percentage Step Size Against End Luminosity for Radius 0.31-0.40m

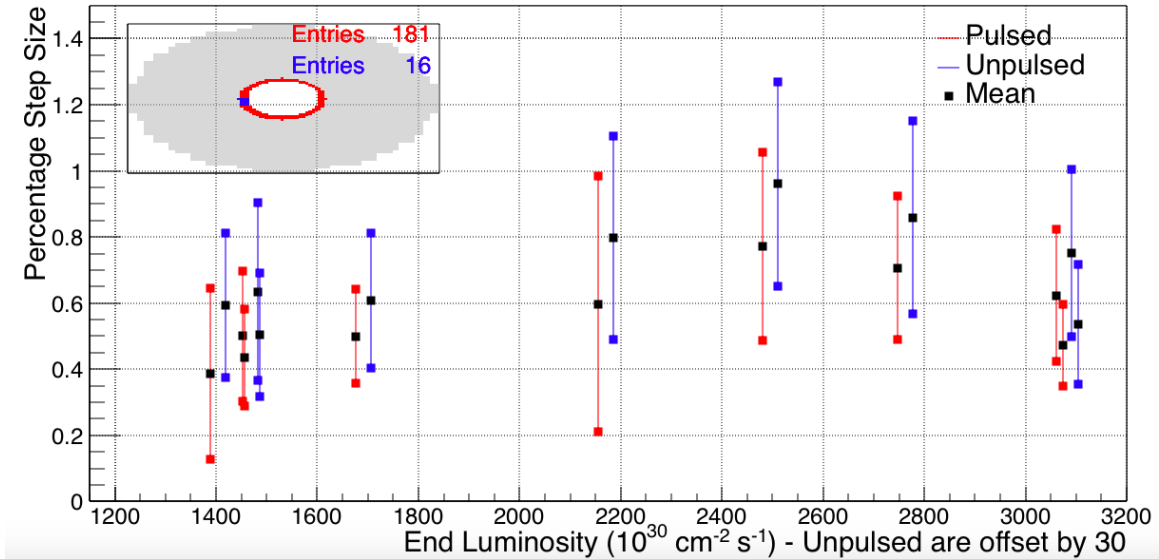


Figure 8.3: Mean and RMS of step size against luminosity ($10^{30} \text{ cm}^{-2} \text{ s}^{-1}$) for radius 0.31-0.40 m in October 2011. Step size is as a percentage of response at end of fill. Inset graph shows which VPTs were used (red are pulsed, blue are unpulsed).

May 2012 Percentage Step Size Against End Luminosity for Radius 0.31-0.40m

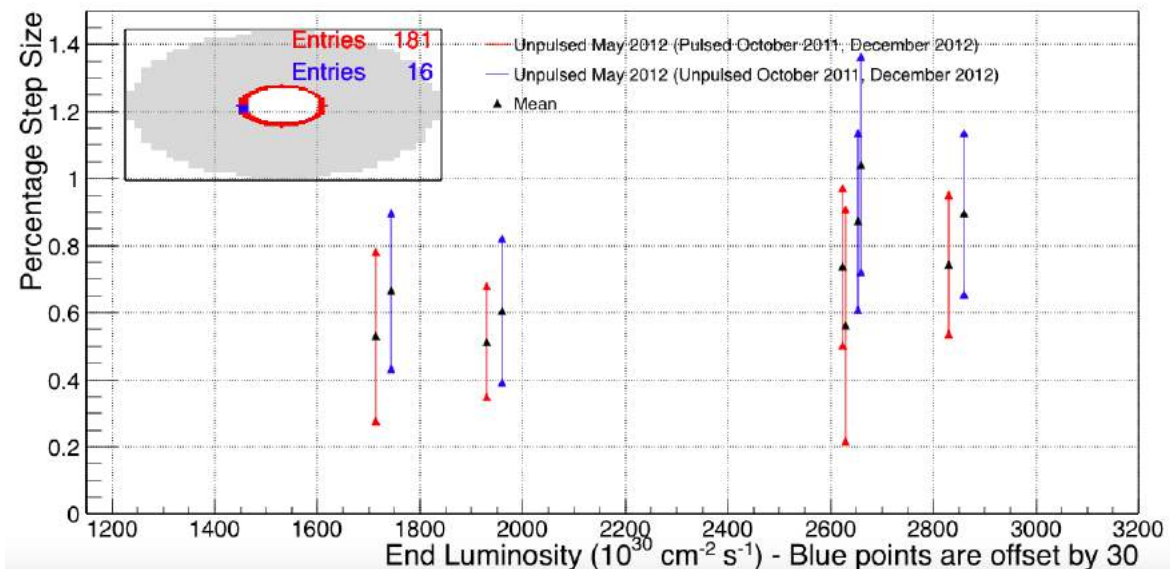


Figure 8.4: Mean and RMS of step size against luminosity ($10^{30} \text{ cm}^{-2} \text{ s}^{-1}$) for radius 0.31-0.40 m in May 2012. Step size is as a percentage of response at end of fill. Inset graph shows which VPTs were used. All VPTS were unpulsed. Red points were pulsed in October 2011 and December 2012, blue were not.

9

Step Size and VPT Photocathode Current

The VPT photocathode current is a useful variable because it allows us to estimate the load experienced by a VPT. It takes into account factors such as VPT position, LHC luminosity and radiation damage in individual crystals and VPTs.

Figure 9.1 shows the VPT step size against end of fill photocathode current for each of the three time periods. The three lines show similarities. In October 2011 the step sizes increase with photocathode current to 0.00325 at 0.2 nA and then begin to plateau, gradually increasing to 0.0045 at 1.4 nA. The May 2012 steps increase to 0.0042 at 0.4 nA and then plateau remaining at 0.0042 until 1.2 nA. The December 2012 steps increase roughly in line with the October 2011 steps, peaking with a step of 0.0035 at 0.3 nA. However, the steps then fall, dropping to 0.0026 at 1.4 nA.

It is important to remember that there is less statistical precision at higher photocathode currents due to the lower numbers of VPTs at large η that receive sufficient radiation, and fewer fills with sufficiently high luminosity. The errors reach 0.0006 above 1 nA for the three time periods.

The October 2011 results, show a strong correlation between step size and photocathode current up to 0.2 nA. This is consistent with our former hypothesis that larger VPT photocathode currents would cause larger steps in response because the change in load that the VPT experiences at the end of fill is larger.

The December 2012 steps decrease for photocathode currents above 0.4 nA. This is unexpected, but is in line with the step size against η plots, where step size decreases towards higher η , and is where the higher photocathode currents are found.

The May 2012 steps, which were unpulsed, are generally larger than the October 2011 and December 2012 steps, which were pulsed. This indicates that the LED pulser may have a stabilising effect. The largest difference is at a photocathode current of 0.5 nA where the step size is approximately 0.001 larger than in October 2011 and December 2012. This is approximately 30% larger than the pulsed October 2011 and December 2012 steps which is significant. However, the pulsed October 2011 steps were 0.002 larger than the pulsed December 2012 steps at a photocathode current of 1.4 nA which is a much bigger difference. The VPTs in both time periods were pulsed so it is possible that other factors

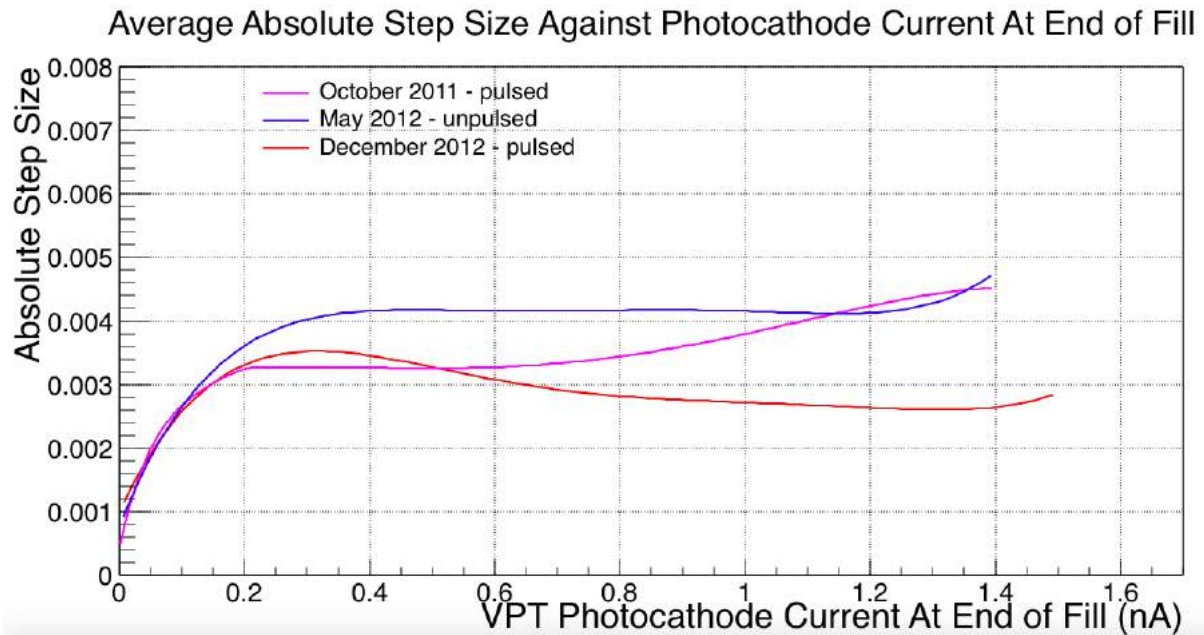


Figure 9.1: Absolute step size against end of fill VPT photocathode current for October 2011 (magenta), May 2012 (blue) and December 2012 (red). The VPTs were pulsed in October 2011 and December 2012 but not in May 2012. VPT photocathode current has units of nA. The response of each channel was normalised to the beginning of operation in 2011. Only the VPTs that were pulsed in October 2011 and December 2012 have been used.

affect step size. Therefore it cannot be concluded with certainty from Figure 9.1 that the lack of LED pulsing was the reason for the larger steps in the May 2012 data.

Figure 9.2 shows how the steps correlate with photocathode current when plotted as a percentage of the channel's response at the end of fill. It shows that both October 2011 and May 2012 percentage steps continue to increase with photocathode current up to 1.3 nA. The May 2012 steps are approximately 0.1 larger than October 2011, above a photocathode current of 0.4 nA. The December 2012 steps increase up to 0.65 and 0.5 nA and then plateau.

Below 0.55 nA, the December 2012 percentage steps were the largest which resulted in the biggest effect on physics results and above 0.55 nA the May 2012 steps were larger. However, all three remained under 0.9 throughout, and the vast majority of VPTs experienced much smaller steps. This includes May 2012 which was unpulsed. These low step sizes are a good result. The fact that the December 2012 steps stop increasing with photocathode current is promising, since future LHC conditions will have higher instantaneous luminosities.

Figures 9.3 and 9.4 show absolute step size, for pulsed and unpulsed VPTs separately, against the VPT photocathode current for October 2011 and December 2012 respectively. These are similar to Figure 9.1, but show the steps for pulsed and unpulsed VPTs separately for a single time period instead of a line for each time period on the same graph, where just the pulsed VPTs for October 2011 and December 2012 were shown. These allow for a comparison between the steps for pulsed and unpulsed VPTs within the same time period and consequently under the same LHC conditions. Figures 9.3 and 9.4 show no substantial differences between the steps for pulsed and unpulsed VPTs within these time periods.

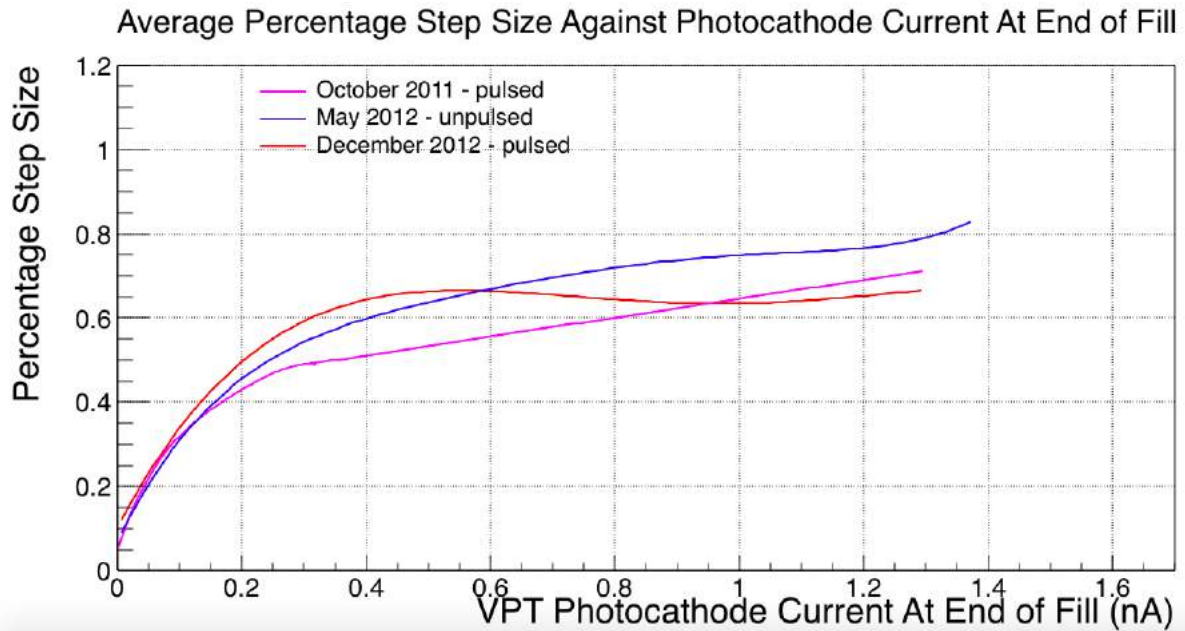


Figure 9.2: Percentage step size against end of fill VPT photocathode current for October 2011 (magenta), May 2012 (blue) and December 2012 (red). The VPTs were pulsed in October 2011 and December 2012 but not in May 2012. VPT photocathode current has units of nA. The step size is as a percentage of the response of the channel at the end of fill. Only the VPTs that were pulsed in October 2011 and December 2012 have been used.

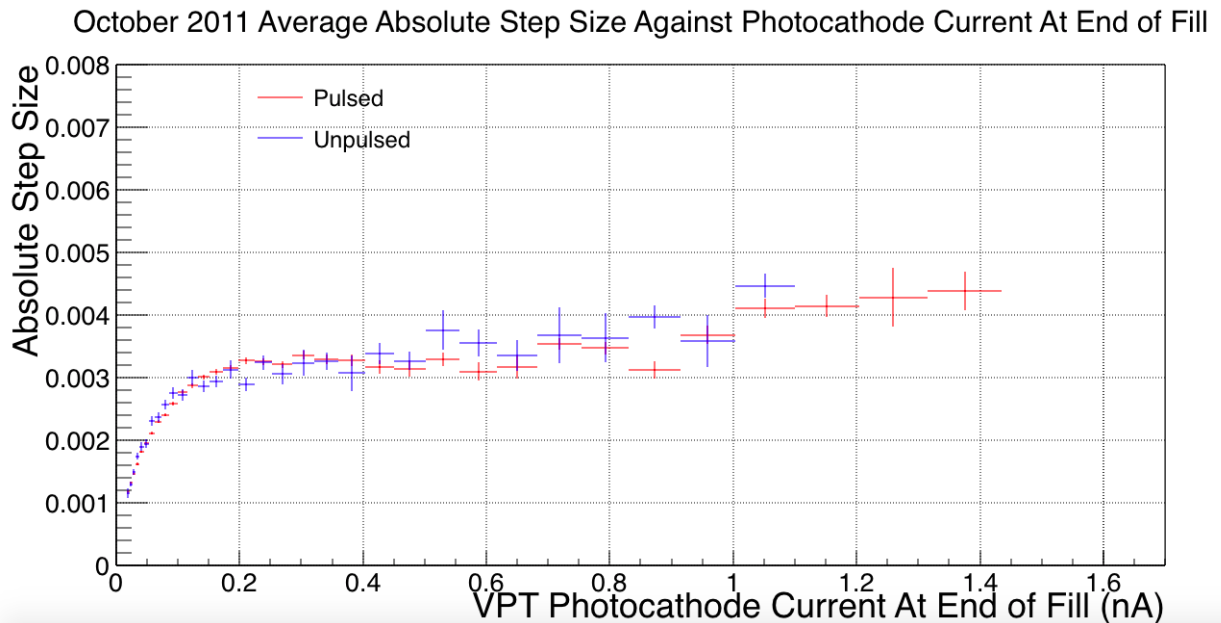


Figure 9.3: Absolute step size against end of fill VPT photocathode current for October 2011 for pulsed (red) and unpulsed (blue) VPTs. VPT photocathode current has units of nA. The response of each channel was normalised to the beginning of operation in 2011.

9.1 Comparison Between Laboratory and LHC

The laboratory tests showed that steps of 1.7% could be reduced to 0.7% using the LED pulser system, as shown in Figure 4.2 [8]. The LHC data from 2011 and 2012 has shown that unpulsed VPTs reach an

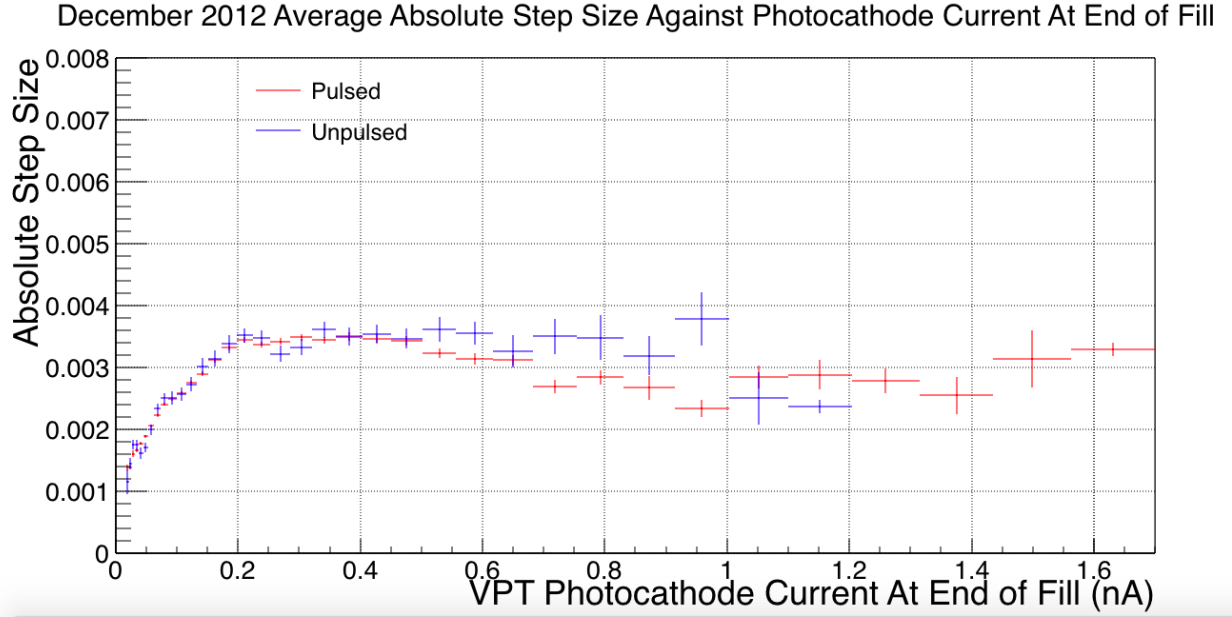


Figure 9.4: Absolute step size against end of fill VPT photocathode current for December 2012 for pulsed (red) and unpulsed (blue) VPTs. VPT photocathode current has units of nA. The response of each channel was normalised to the beginning of operation in 2011.

average step of 0.85% at the highest photocathode currents and 0.7% for pulsed VPTs. These values are smaller than the laboratory results and are only concern a small number of VPTs at the very centre of EE+. The vast majority of VPTs have steps considerably below these levels.

An interesting observation is that the steps are in different directions between the lab and the CMS experiment. In the laboratory the response dropped at the end of a fill, as shown in Figure 4.2, whereas it increased with the LHC data, as seen in Figure 1.6. It is currently unclear why this difference occurs.

The laboratory experiment aimed to replicate conditions in the LHC at a luminosity of $10^{34} \text{ cm}^{-2} \text{ s}^{-1}$, whereas the 2011 and 2012 data from the LHC have final luminosities from 1.4 to $5.2 \times 10^{33} \text{ cm}^{-2} \text{ s}^{-1}$. This is a factor of between two and seven times smaller than in the laboratory. However, the absolute step sizes in CMS all plateau to a value of 0.3 to 0.4% for photocathode currents above 0.3 to 0.4 nA. This suggests that there may not be a monotonically increasing step size with luminosity which bodes well for future LHC operation.

10

Spread of Step Sizes

The laboratory tests found a large step of 1.7% for an unpulsed VPT and a large reduction in step size to 0.7%, when pulsed, for only one of the five tested VPTs [8]. A smaller difference was observed in one other VPT but not in the three remaining VPTs. So far, this report has looked at average step sizes for different groupings of VPTs. It is interesting to look at the spread of step sizes in LHC data. It is possible that only some VPTs experience large steps when unpulsed but that the majority do not. The number of VPTs experiencing large steps were investigated by plotting the distributions of step size for pulsed and unpulsed VPTs, as shown in Figure 10.1

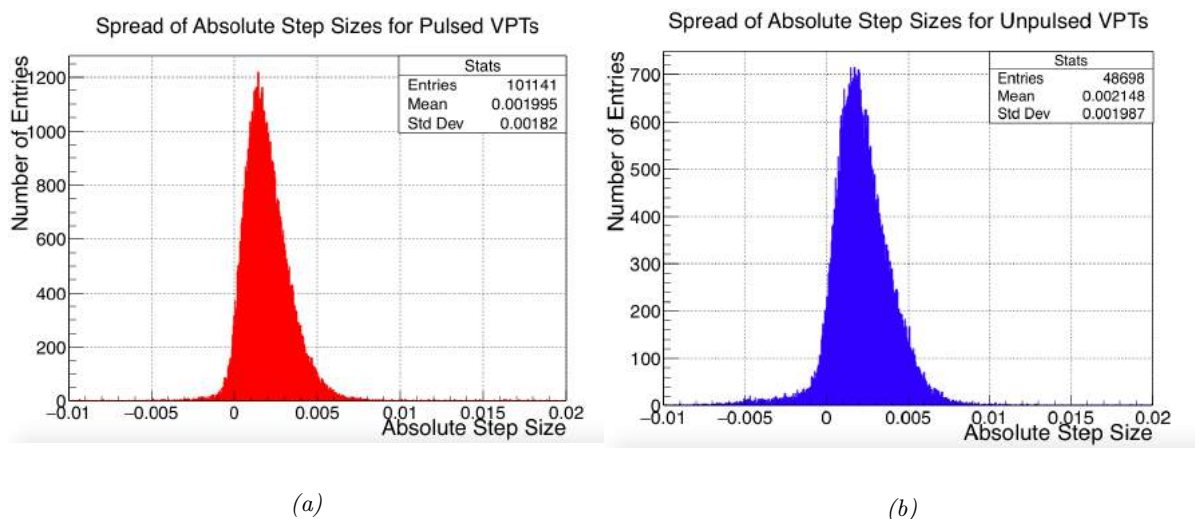


Figure 10.1: Spread of absolute step sizes for pulsed (left, red) and unpulsed (right, blue) VPTs for the fills investigated in October 2011, May 2012 and December 2012. The response of each channel was normalised to the beginning of operation in 2011.

The distributions for absolute step size are shown in Figure 10.1. The distributions for pulsed and unpulsed VPTs are similar. The mean step size for unpulsed VPTs is only slightly higher, at 0.0021

compared to 0.0020 for pulsed VPTs. The majority of the unpulsed steps are from May 2012, where all VPTs were unpulsed. All pulsed steps are from October 2011 and December 2012 where the majority of VPTs were pulsed.

The standard deviation of unpulsed percentage steps is slightly higher, at 0.0020 compared to the pulsed VPTs, at 0.0018. However, this is a small difference.

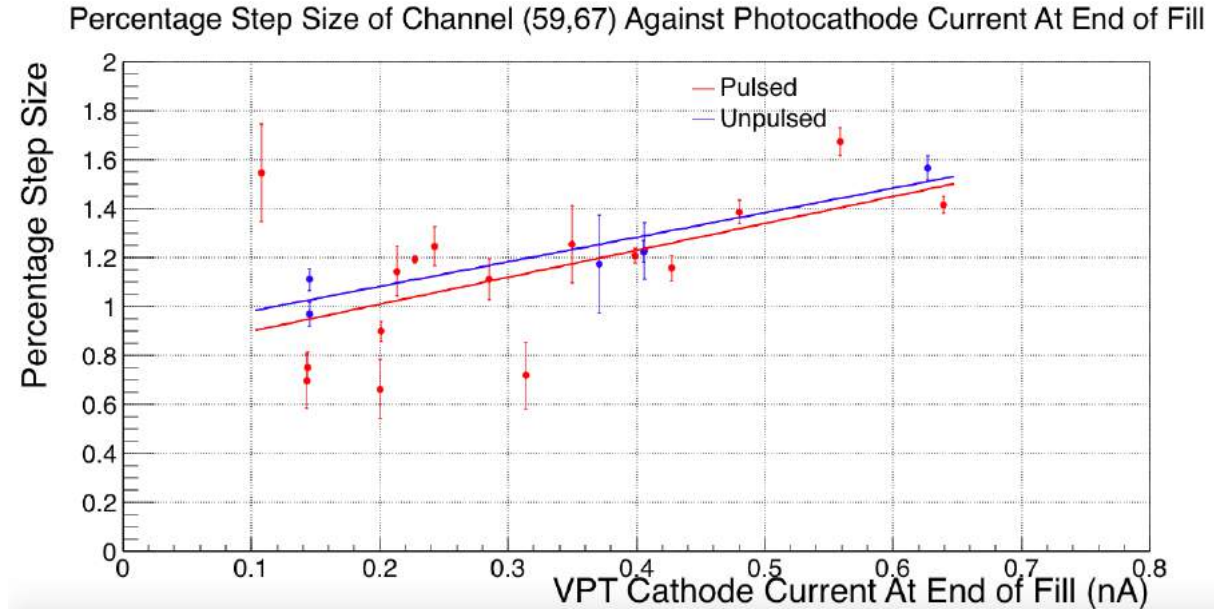


Figure 10.2: Percentage step size against end-of-fill photocathode current for the VPT at (59,67) in EE+. Pulsed points, from October 2011 and December 2012, are ref. Unpulsed points, from May 2012 are blue. Step size is as a percentage of the channel's response at the end of the fill.

About 20 VPTs experienced a percentage step size above 1.5%, in the unpulsed May 2012 period. The percentage step size against the end-of-fill photocathode current, for one of these VPTs, is shown in Figure 10.2, using data from the October 2011, May 2012 and December 2012 periods. The percentage step size, from the linear fit, increases by approximately 65% with photocathode current. The data show no significant difference between pulsed and unpulsed steps.

Figure 10.3 shows the results for the same VPT as in Figure 10.2 but for absolute step size. It shows a positive correlation between absolute step size and end-of-fill photocathode current. The absolute step size from the fits increases by approximately 35% for the pulsed data and approximately 50% for the unpulsed data.

Figure 10.3 shows that the VPT experienced slightly larger absolute steps when unpulsed in May 2012, compared to when pulsed in October 2011 and December 2012. This is consistent with Figure 9.1 which showed the average absolute step size, for all VPTs, against the photocathode current for each time period. The larger steps may be caused by a difference in other conditions between the different time periods and not by the lack of LED pulsing.

The plots in Figures 10.2 and 10.3 are specific to one VPT but the other ~ 20 VPTs with high steps in this sample presented similar general results.

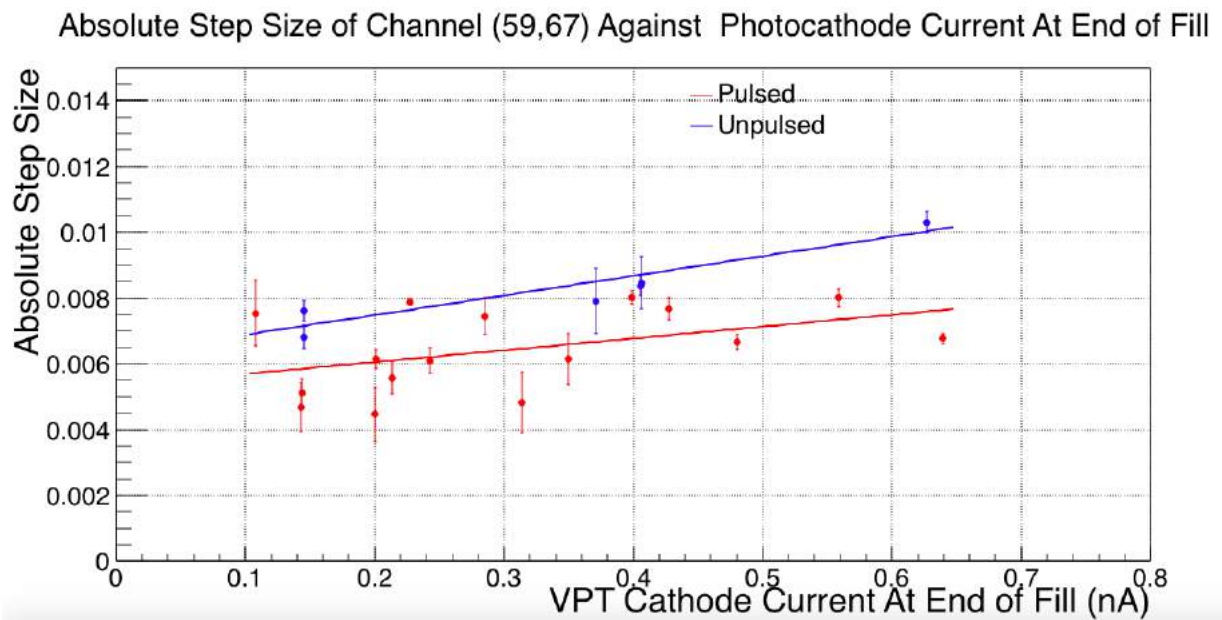


Figure 10.3: Absolute step size against end-of-fill photocathode current for the VPT at (59,67) in EE+. Pulsed points, from October 2011 and December 2012, are red. Unpulsed points, from May 2012 are blue. The response of the channel was normalised to the beginning of operation in 2011.

11

Conclusion

Data from the LHC in October 2011, May 2012 and December 2012 have been used to calculate the steps in the response of VPTs in EE+ at the end of fills and to investigate the effect of the LED stability pulsers in reducing the steps. October 2011 and December 2012 had LED pulsing for the majority of VPTs. The May 2012 data were unpulsed, allowing for a comparison between pulsed and unpulsed VPTs in the different datasets. Additionally, a small number VPTs in October 2011 and December 2012 were unpulsed, allowing for comparisons between pulsed and unpulsed VPTs within the same fill, under the same LHC conditions.

The results have been compared to laboratory measurements which found steps of 1.7% in response for one unpulsed VPT which were reduced to 0.7% with pulsing. The steps from LHC data were found to be smaller than in the laboratory. The stability pulsers were found to have little, if any, effect in reducing step size.

The October 2011 and May 2012 data showed that step size increased with pseudorapidity, towards the centre of the endcap, suggesting that the LHC radiation load is an important factor as it increases with pseudorapidity.

The December 2012 data disagreed with the results. The step size increased up to $\eta=2.35$ and then decreased. It is unclear why this would be the case as photocathode current continued to increase with η . The point where the decrease in step size begins is the point where the crystal producer changes. There is a possibility, therefore, that the step in response may not be solely due to the VPTs.

The average step size did not correlate with the end of fill instantaneous luminosity. This appears to contradict the previous results which showed that step size was affected by the load on the VPT.

However, step size was found to only initially increase with photocathode current and then plateau, showing that step size does not increase significantly for larger photocathode currents. This might explain the lack of correlation between step size and end of fill luminosity.

The May 2012 absolute steps, which were unpulsed, were approximately 20% larger than the pulsed October 2011 and December 2012 steps, for photocathode currents between 0.3 and 0.8 nA. This could suggest that the LED pulsing has had a stabilising effect. This is somewhat supported by plots comparing step size and photocathode for single VPTs which also showed the unpulsed steps to be approximately 20% larger than the pulsed, for photocathode currents between 0.1 and 0.6 nA. However,

at photocathode currents above 1.1 nA, the unpulsed May 2012 and pulsed October 2011 average steps for all VPTs were equal in size, and approximately 45% larger than the pulsed December 2012 steps.

The May 2012 difference may not have been caused by the lack of pulsing. This is supported by looking at the difference between pulsed and unpulsed VPTs within the same fill. No significant difference in step size between pulsed and unpulsed VPTs is observed in these plots.

The most important observation from this work is that the step size comes to a plateau for photocathode currents above ~ 0.5 nA. This is very important for future LHC operation where higher luminosities, and therefore higher photocathode currents, are expected.

The average percentage step size, for both pulsed and unpulsed VPTs, was approximately 0.4% for a photocathode current of 0.2 nA. This is below the physics requirement of minimising the impact on energy resolution to less than 0.5%. The average step size only reached approximately 0.7% when photocathode currents increased to 1.3 nA, which is still close to the 0.5% requirement. In addition, the steps are fast and occur well within the 40 minute cycle time for laser pulsing. Some steps were observed to have taken place within four minutes of end of fill. As a consequence any affected data is only a very small fraction of an LHC fill, which usually last for more than eight hours. We conclude that the VPT steps in response will only minimally affect physics at the LHC.

Bibliography

- [1] The ATLAS Collaboration. *Observation of a New Particle in the Search for the Standard Model Higgs Boson with the ATLAS Detector at the LHC*, CERN-PH-EP-2012-218
- [2] The CMS Collaboration. *Observation of a new boson at a mass of 125 GeV with the CMS experiment at the LHC*, CERN-PH-EP/2012-220 2013/01/29
- [3] Parcly Taxel, CC BY-SA 3.0, <https://commons.wikimedia.org/w/index.php?curid=28638463>
- [4] CERN Document Server. CMS-PHO-EVENTS-2013-004, <https://cds.cern.ch/record/1606506?ln=en> Accessed 04/05/2016
- [5] CERN Document Server. CMS-PHO-EVENTS-2012-003, <https://cdsweb.cern.ch/record/r1459462/> Accessed 21/04/2016
- [6] CERN Document Server. CMS-PHO-EVENTS-2012-004, <https://cdsweb.cern.ch/record/1459462/> Accessed 21/04/2016
- [7] A. Benaglia. *Journal of Instrumentation*, VOL.9, C02008 (2014), ISSN 17480221, [http : //stacks.iop.org/1748 - 0221/9/i = 02/a = C02008](http://stacks.iop.org/1748-0221/9/i=02/a=C02008).
- [8] A. Ledovskoy. *Stabilizing Effects of 100 Hz Pulsing on VPTs @ UVa*, JUNE 2010 [https : //indico.cern.ch/event/99354/contribution/7/attachments/1121207/1599965/100624_ee_ledovskoy.pdf](https://indico.cern.ch/event/99354/contribution/7/attachments/1121207/1599965/100624_ee_ledovskoy.pdf)
- [9] CMS Collaboration. *CMS Technical Design Report, Volume II: Physics Performance*, J. Phys. G: Nucl. Part. Phys 34 995-1579 (2007)
- [10] CERN Document Server. CMS-PHO-GEN-2016-001, <https://http://cds.cern.ch/record/2120661> Accessed 14/05/2016
- [11] CMS Collaboration. *The CMS experiment at the CERN LHC*, JOURNAL OF INSTRUMENTATION, VOL3, AUGUST 2008
- [12] CMS Collaboration. *The Electromagnetic Calorimeter Project: Technical Design Report*, CERN/LHCC-97-33, CMS-TDR 4 (1997)
- [13] D.J.A Cockerill. *The CMS Electromagnetic Calorimeter at the LHC*, 34TH INTERNATIONAL CONFERENCE ON HIGH ENERGY PHYSICS, PHILADELPHIA, (2008)
- [14] G. Dissertori et al. *Radiation damage kinetics in PbWO₄ crystals*, CMS Note 1997/009
- [15] R M Brown *EE Photodetectors for SLHC*, FNAL 20/1108 (2008), Sides 10-13
- [16] P. Hobson. *The stability of vacuum phototriodes to varying light pulse loads and long term changes in response*, JUNE 2012
- [17] K. W. Bell et al. *Vacuum Phototriodes for the CMS Electromagnetic Calorimeter Endcap*, IEEE TRANSACTION ON NUCLEAR SCIENCE, VOL.51, NO. 5, OCTOBER 2004

- [18] CMS Collaboration. *ECAL detector performance plots*, CMS-DP-2013/007 (2012), https://twiki.cern.ch/twiki/pub/CMSPublic/EcalDPGResultsCMSDP2013007/histories_2011-2012.pdf
- [19] Dawn Elizabeth Leslie. *The effect of pulse rate on VPT response and the use of an LED light to improve stability*, ICMS CR -2009/284 (2008)
- [20] A Ledovskoy *Photo-Statistics in EE* JUNE 2015 https://indico.cern.ch/event/395438/contribution/1/attachments/792251/1085990/150618_dpg_ledovskoy.pdf
- [21] <http://cmslxr.fnal.gov/source/DataFormats/EcalDetId/interface/EEDetId.h#0070>

Appendix A

VPT Encoding

The following formulae are used to determine the position of each VPT on the detector from its unique eight digit hexadecimal ID number for that channel [21]:

$$ix = ((ID) \gg 7) \& 0x7F \tag{A.1}$$

$$iy = ((ID) \& 0x7F) \tag{A.2}$$

$$z = ((ID) \& 0x4000) ? (1) : (-1) \tag{A.3}$$

Appendix B

Data and Plot Generating Scripts

Table B.1 shows the scripts used to generate the plots used in this report. Table B.2 shows the data files and scripts used to estimate the VPT response step sizes and the end of fill VPT photocathode currents for the three time periods.

Figure	Script Name
6	JumpExample.C
23	PlotUnpulsedRegions.C
24	2011.C - PlotLumi()
25	2012.C - PlotLumi()
26	May2012.C - PlotLumi()
27	2011.C - CheckFit(42,42)
28	StepandCurrentVEta.C
29	StepandCurrentVEta.C
30	StepandCurrentVEta.C
31	2012.C - CheckFit(50,39)
33	AllYearsStepVLumi.C
34	2011StepVLumi.C
35	May2012StepVLumi.C
36	StepVCurrent.C
37	StepVCurrent.C
38	SingleYearStepVCurrent.C
39	SingleYearStepVCurrent.C
40	Spread.C
41	SingleVPTStepVCurrent.C
42	SingleVPTStepVCurrent.C

Table B.1: Names of the scripts used to generate plots in this report

Data	October 2011	May 2012	December 2012
Instantaneous LHC Luminosity Data	2011LumiData.txt	May2012LumiData.txt	2012LumiData.txt
Laser Monitoring Data	2011ecal_laser_dumped_ids.dat	May2012ecal_laser_dumped_ids_EE.dat	2012ecal_laser_dumped_ids_EE.dat
Anode Currents	2011AnodeCurrents.txt	May2012AnodeCurrents.txt	2012AnodeCurrents.txt
Step Size Estimates	2011.C	May2012.C	2012.C
VPT Photocathode Current Estimates	2011Currents.C	May2012Currents.C	2012Currents.C

Table B.2: Data files and scripts used to estimate VPT step sizes and photocathode currents